NTNU
Norwegian University of
Science and Technology

Electron-phonon coupling in graphene

Kristian Framhus Hole-Drabløs

Master of Science in Physics and Mathematics
Submission date: June 2018
Supervisor: Asle Sudbø, IFY

Norwegian University of Science and Technology
Department of Physics

Abstract

The aim of this Master thesis was to perform a theoretical study of the electron-phonon coupling in graphene. The main results of the thesis are the electron-phonon coupling constant as a function of the Fermi energy, a derivation of the phonon dispersion and a calculation of the band structure. It is shown that the electron-phonon coupling constant is correlated with the density of states, which makes it highly dependent on the electron bands. The calculated band structure is in good agreement with literature. For the phonon dispersion, the quantitative shape matches known results, but lacks some of the details. Despite the lack of details in the dispersion, it is considered sufficient for calculating the electron-phonon coupling, as the coupling is mostly determined by the band structure.

Sammendrag

Hensikten med denne masteroppgaven har vært å gjennomføre en teoretisk studie av elektron-fonon-kobling i grafen. Hovedresultatene i oppgaven er elektron-fonon-koblingskonstanten som funksjon av Fermienergien, en utledning av fonondispersjonen og en beregning av båndstrukturen. Det vises at formen til elektron-fonon-koblingskonstanten følger formen til tettheten av tilstander i båndstrukturen svært tett. Båndstrukturen stemmer godt overens med eksisterende resultater. Formen til fonondispersjonen er lik formen til eksisterende resultater, men detaljene er forskjellige. Ettersom det primære målet med fonondispersjonen er å beregne elektron-fonon-koblingskonstanten, som er svært avhengig av båndstrukturen, anses modellen som brukes som god nok til sitt formål.

Preface

This Master thesis was written during the spring semester of 2018 and marks the end of my Master of Science degree in *Physics and Mathematics* at the Norwegian University of Science and Technology (NTNU). The thesis is a study of the electron-phonon coupling in graphene. I would like to thank my supervisor, professor Asle Sudbø, for triggering my curiosity and always finding time for my questions. For that I am very grateful. I would also like to thank my girlfriend Yngvild Hamre for bringing sunshine into my life.

Kristian Hole-Drabløs
Trondheim, Norway
June 2018

Contents

Chapter 1

Introduction

1.1 Graphene - a remarkable material

The pencil, an effective tool used for communication and art, has been commonly used since the 16th century [1], but in recent years its popularity has decreased as digital tools have emerged. Thus some label pencils as simple, boring, and out of date. The discussion about whether pencils are to stay or not will not be taken here, the focus will rather be on the truly remarkable and highly disruptive physics contained in a simple, gray pencil mark. In 2004, a research group at the University of Manchester lead by A. Geim and K. Novoselov was able to pick graphite apart, layer by layer, thus creating the first two-dimensional crystalline material, graphene [2]. For the discovery of graphene and exhaustive investigations of its properties [3], they shared the Nobel prize in 2010.

Even though graphene is a simple honeycomb lattice of carbon atoms, it shows extraordinary properties which outperforms much more complex materials in many respects. Among the mechanical properties is an immense in-plane strength [4], a Young's modulus of 1000GPa (for comparison, high-strength concrete has 30GPa and steel up to 200GPa [5]), and a high thermal

conductivity [6]. Among the electrical properties are great electron mobility [7] and the ability to sustain extremely high densities of electrical current [8], up to a million times more than copper. Another interesting property is that graphene shows impermeability to any gases [9], thus it is a highly interesting material for hydrogen storage [10, 11].

From a theoretical physicist's point of view, perhaps the most interesting aspect arise from the electron dispersion [3, 12]. At two distinct points in the electronic spectrum, Dirac cones form [13], i.e. the electron dispersion is linear in momentum. The electrons behave as massless relativistic particles, known as Dirac fermions, and show exceptional transport properties [14]. Due to this, the quantum Hall effect has been observed at room temperature [15]. As the quantum Hall effect is a purely quantum mechanical effect, one would assume it to require extreme conditions to be observable, e.g. by using a cold atom system. Thus the discovery of the effect at room temperature in graphene marked the start of a new paradigm in two-dimensional electron physics, taking it from low-temperature laboratories to the real world [16].

Recently, in March 2018, the Jarillo-Herrero group at MIT published two papers, in which they reported bi-layer graphene to be an unconventional superconductor and exhibit Mott-like states [17, 18]. The transition temperature to the superconducting state was reported to be $1.3K$, which is, surprisingly, a remarkably high temperature given the low carrier density [19]. An additional observation that supports labelling graphene as an unconventional superconductor is the similarity of the temperature-carrier-density phase diagram to the one obtained for cuprates [17], copper oxides known to be unconventional superconductors. The research on high-temperature superconductors has the last three decades focused on cuprates, but without promising results [20], as the unconventional pairing is not fully understood.

As graphene has a simple form and is highly tuneable, it is an ideal platform for studying strongly correlated phenomena and quantum effects. By gaining a better understanding of them, one might gain insights in the physics of high-temperature superconductors and quantum spin liquids [17]. The discovery of superconductivity in bi-layer graphene might be the trigger behind

the development of a theory of unconventional superconductors and room temperature superconductivity. These are truly exciting times!

1.2 The aim and structure of the thesis

Solids can be divided into two subsystems, an electron and a phonon system. In this thesis, properties of the two subsystems of graphene are investigated, both as stand-alone systems and as a single coupled system. The main result of the thesis is the dependency of the electron-phonon coupling constant of the Fermi energy in the low temperature limit, which is presented in section 5.3.3. In addition, the band structure and phonon dispersion, presented in section 5.1 and 5.2, are important results. Two key questions to answer will be how much the different electron bands couple to the different phonon modes, and if there are any band transitions that dominate the electron scattering process.

The structure of the thesis is as follows. In chapter 2 mathematical conventions and a short introduction to second quantization is presented. Chapter 3 contains derivations of the models applied in the thesis. A brief introduction to graphene is given in chapter 4. In chapter 5 the models of chapter 3 are specialized to graphene and relevant properties are calculated. Concluding remarks are given in chapter 6.

Chapter 2

Preliminaries

2.1 Mathematical conventions

In this master thesis a mathematical convention common in the physics community will be used. Vectors will be bald faced, like the wave vector $\mathbf{k}$ and the position vector $\mathbf{r}$, where the Cartesian unit vectors are exceptions as they are denoted with a hat, $\hat{x}, \hat{y}, \hat{z}$. Scalars, complex or real, will be denoted with a normal symbol, e.g. z, and the complex conjugate with an asterisk, z^*.

The Hermitian conjugate will be emphasized with a dagger, as in $\psi^\dagger$. Matrices written out in component form will be enclosed by brackets. The commutation relation between A and B is written with square brackets, $[A,B] = AB - BA$, while the anti-commutator is written with curly brackets, $\{A,B\} = AB + BA$. The curly brackets will also denote a set of variables or values, e.g. $\{\alpha,\beta\} = \{x,y,x\}$ and $i = \{1,2,3\}$. It will be clear from the context which interpretation of the curly brackets that is intended; when operators are inside the brackets it is an anti-commutator, otherwise it denotes a set. A sum over two sum indices where they are not suppose to be equal are written $\sum_{i\neq j}$, as a short notation for $\sum_{i,j,i\neq j}$.

The creation and annihilation operators will mostly be denoted by $c_\lambda^{(\dagger)}$, but also by $\left(c_\lambda^{(\dagger)}\right)^A$ and $\left(c_\lambda^{(\dagger)}\right)^B$, depending on the context. The subscript of the operators will typically be written $c_{\mathbf{k}\alpha}^{(\dagger)}$, but sometimes it will be separated by a comma, e.g. $c_{\mathbf{k}+\mathbf{q},\alpha}^{(\dagger)}$.

2.2 Second quantization

In 1927, P. Dirac introduced a new mathematical approach to describe QED[1] systems [21]. The mathematical approach was within a few years adapted by the community which has since then developed it to what is now known as the second quantization formalism. The technique is adapted from quantum field theory where particles are interpreted as excitations of fields and the traditional wave function is replaced by occupation number states. In the occupation number representation a state is written as $|N\rangle = \left|n_{\lambda_1}, n_{\lambda_2}, ...\right\rangle$, where there are n_{λ_i} particles in state λ_i and in total N particles. In second quantization, creation and annihilation operators, $c_{\lambda_i}^\dagger$ and c_{λ_i}, play a central role as they create or remove a particle from state λ_i.

$$c_{\lambda_i}\left|n_{\lambda_1}, n_{\lambda_2}, ..., n_{\lambda_i}, ...\right\rangle = \sqrt{n_{\lambda_i}}\left|n_{\lambda_1}, n_{\lambda_2}, ..., n_{\lambda_i} - 1, ...\right\rangle \tag{2.2.1}$$

$$c_{\lambda_i}^\dagger\left|n_{\lambda_1}, n_{\lambda_2}, ..., n_{\lambda_i}, ...\right\rangle = \sqrt{n_{\lambda_i} + 1}\left|n_{\lambda_1}, n_{\lambda_2}, ..., n_{\lambda_i} + 1, ...\right\rangle \tag{2.2.2}$$

A many-body state can be created by employing creation operators to the vacuum state:

$$\prod_{i=1}\left(c_{\lambda_i}^\dagger\right)^{n_{\lambda_i}}|0\rangle = \left|n_{\lambda_1} n_{\lambda_2} ... n_{\lambda_l} ...\right\rangle = |N\rangle\,. \tag{2.2.3}$$

In the same manner, the vacuum state can be created by employing annihilation operators on a given state

[1] Quantum electrodynamics

$$\prod_{i=1}\left(c_{\lambda_i}\right)^{n_{\lambda_i}}|N\rangle=\prod_{i=1}\left(c_{\lambda_i}\right)^{n_{\lambda_i}}.\left|n_{\lambda_1}n_{\lambda_2}...n_{\lambda_l}...\right\rangle=|0\rangle \tag{2.2.4}$$

For bosons there are no restrictions on the occupation number of a state, except that it has to be a non-negative integer. In fact, all the particles could in principle be in the same state. Fermions on the other hand, as they follow the Pauli principle, are restricted to 0 or 1. Hence, applying a creation operator to an already occupied fermionic state will annihilate the many-body state. As bosons behave symmetrically and fermions anti-symmetrically with respect to interchange of particle indices, it can be shown [22] that the following commutation and anti-commutation relations holds:

$$\begin{aligned}
&[c_\lambda,c_{\lambda'}]=0 && \{c_\lambda,c_{\lambda'}\}=0\\
&[c^\dagger_\lambda,c^\dagger_{\lambda'}]=0 && \{c^\dagger_\lambda,c^\dagger_{\lambda'}\}=0\\
&[c_\lambda,c^\dagger_{\lambda'}]=\delta_{\lambda\lambda'} && \{c_\lambda,c^\dagger_{\lambda'}\}=\delta_{\lambda\lambda'}
\end{aligned} \tag{2.2.5}$$

where the left-hand-side panel is for bosons and the right for fermions. { , } denotes anti-commutators.

All operators can be expressed in terms of creation-annihilation-operator pairs in the second quantization formalism. Operators will either be single-particle or two-particle operators, where single and two refer to the number of creation-annihilation pairs involved. If the first-quantized form of an operator $\hat{O}_1=\sum_i\hat{O}_1(\mathbf{r_i})$ is known, the second quantized form is obtained via

$$\begin{aligned}
O_1&=\sum_{\lambda,\mu}\langle\lambda|\hat{O}_1|\mu\rangle\,c^\dagger_\lambda c_\mu\\
&=\int\mathrm{d}\mathbf{r}\sum_{\lambda,\mu}\psi^*_\lambda(\mathbf{r})\hat{O}_1(\mathbf{r})\psi_\mu(\mathbf{r})c^\dagger_\lambda c_\mu\\
&=\int\mathrm{d}\mathbf{r}\,\hat{\psi}^\dagger(\mathbf{r})\hat{O}_1(\mathbf{r})\hat{\psi}(\mathbf{r}),
\end{aligned} \tag{2.2.6}$$

where the field operators $\hat{\psi}^\dagger(\mathbf{r}),\hat{\psi}(\mathbf{r})$ have been introduced and the specie index is suppressed. The field operators are expressed in terms of a linear combination of creation/annihilation operators projected onto the basis

vectors, $\psi_k(\mathbf{r})$, where k is the set of quantum numbers that describes the system [22]:

$$\hat{\psi}^{(\dagger)}(\mathbf{r}) \equiv \sum_k \psi_k(\mathbf{r})^{(\dagger)} c_k^{(\dagger)}. \tag{2.2.7}$$

In the same manner, the second quantized version of a two-particle operator $O_2 = \sum_{i \neq j} \hat{O}_2(\mathbf{r_i}, \mathbf{r_j})$ is

$$\begin{aligned} O_2 &= \sum_{\lambda,\mu,\gamma,\nu} \langle \lambda\mu | \hat{O}_2 | \gamma\nu \rangle c_\lambda^\dagger c_\mu^\dagger c_\gamma c_\nu \\ &= \int \mathrm{d}\mathbf{r}\, \mathrm{d}\mathbf{r}'\, \hat{\psi}^\dagger(\mathbf{r}) \hat{\psi}^\dagger(\mathbf{r}') \hat{O}_2(\mathbf{r}, \mathbf{r}') \hat{\psi}(\mathbf{r}') \hat{\psi}(\mathbf{r}) \end{aligned} \tag{2.2.8}$$

where the matrix elements are

$$\langle \lambda\mu | \hat{O}_2 | \gamma\nu \rangle = \int \mathrm{d}\mathbf{r_1}\, \mathrm{d}\mathbf{r_2}\, \psi_\lambda^*(\mathbf{r_1}) \psi_\mu^*(\mathbf{r_2}) \hat{O}_2 \psi_\gamma(\mathbf{r_2}) \psi_\nu(\mathbf{r_1}).$$

In condensed matter physics, the system is often described as a lattice, which makes it convenient to pick the lattice points as the basis λ. Due to the periodicity of lattices, the Fourier transform of the operators, $c_\mathbf{k}$ and $c^\dagger{}_\mathbf{k}$, is introduced

$$\begin{aligned} c_{\mathbf{r_i}} &= \frac{1}{\sqrt{N}} \sum_\mathbf{k} c_\mathbf{k} e^{i\mathbf{k}\mathbf{r_i}} \\ c_{\mathbf{r_i}}^\dagger &= \frac{1}{\sqrt{N}} \sum_\mathbf{k} c_\mathbf{k}^\dagger e^{-i\mathbf{k}\mathbf{r_i}}, \end{aligned} \tag{2.2.9}$$

where N is the number of lattice sites in real space, $\mathbf{r_i}$ is the position of lattice site i and the sum over $\mathbf{k}$ runs over the first Brillouin zone. In addition, the relation

$$\frac{1}{N} \sum_{j=1}^{N} e^{-i(\mathbf{k}-\mathbf{k}')\mathbf{r_j}} = \delta_{\mathbf{k}\mathbf{k}'}, \tag{2.2.10}$$

is very useful.

Chapter 3

The Fröhlich Hamiltonian

A perfect solid is made up of a lattice of atoms and electrons. In practice, there will be some impurities in the lattice and some surface effects due to the finite size of the crystal, they are however neglected here. Hence it is convenient to divide the solid into two connected subsystems. The aim of this section is to present a Hamiltonian that describes such a system and in addition is suited for a perturbative treatment. The Fröhlich Hamiltonian is precisely such a Hamiltonian

$$\hat{H} = \hat{H}_{\text{el}} + \hat{H}_{\text{ph}} + \hat{H}_{\text{el+ph}}. \tag{3.0.1}$$

It was originally introduced by H. Fröhlich in the 1950s to describe a conduction electron in an ionic crystal, basically a polaron [23]. In this thesis it will be used to describe a solid, a coupled system of electrons and phonons. The coupling term will be treated as a perturbation to the exactly solvable non-interacting electron and phonon parts.

In section 3.1, a tight-binding model for the electrons is derived. Section 3.2 contains a derivation of the phonon Hamiltonian, considering up to next

nearest neighbour ion interactions. Finally, in section 3.3, the electron-phonon coupling is introduced.

3.1 A tight-binding model for electrons

Due to bonding between lattice sites, (some of) the electrons of a solid are said to be localized, making it convenient to describe them using tight-binding models. Such models assume that the electrons are constrained to a small region in the vicinity of their respective atoms, hence limiting the range of interaction to a small neighbourhood around the lattice sites. The first attempt to describe solids using a tight-binding model was introduced by F. Bloch in 1928 [24], where he approximated the wave functions by s orbitals of the different lattice sites. In 1934, H. James, N. Mott and H. Skinner made a huge improvement to Bloch's model when they took different atomic orbitals into account [25]. This 1934 model laid the foundation of the model which is used in this thesis, the LCAO[1] method. It was introduced by J. Slater and G. Koster in the important 1954 paper [26]. The key idea is that a superposition of the wave functions from isolated atoms is sufficient to describe the electronic band structure of a solid.

The crystal potential is determined by the sum of the potential stemming from the atom of the lattice

$$V(\mathbf{r}) = \sum_{j=1}^{N} \sum_{i=1}^{n} V_{\mathrm{at},i}(\mathbf{r} - \mathbf{R}_j - \boldsymbol{\tau}_i), \tag{3.1.1}$$

where j runs over the unit cells, i over the atoms in each unit cell, $V_{\mathrm{at},i}$ is the potential of a single atom of type i, $\mathbf{R}_j$ gives the position of unit cell j and $\boldsymbol{\tau}_i$ denotes the relative position of atom i within the unit cell. The resulting crystal Hamiltonian is

$$\hat{H} = -\nabla^2 + V(\mathbf{r}). \tag{3.1.2}$$

[1] Linear Combination of Atomic Orbitals

The aim is to link the electron wave function to the atomic orbitals, which satisfy the Schrödinger equation

$$\left(-\nabla^2 + V_{\mathrm{at},i}\right)\phi_{ni} = \mathcal{E}_{ni}\phi_{ni}, \tag{3.1.3}$$

where ϕ_{ni} is the n'th orbital of atom type i and $\mathcal{E}_{ni}$ its associated energy. As the tight-binding model will be applied to graphene, which is only made up of carbon atoms, the lable i is omitted from the potential and the orbitals. Due to the periodicity of the lattice, the wave functions will be Bloch waves [27]

$$\Phi_{\mathbf{k}}(\mathbf{r}) = e^{i\mathbf{kr}}u_{\mathbf{k}}(\mathbf{r}), \tag{3.1.4}$$

where $u_{\mathbf{k}}(\mathbf{r})$ has the same periodicity as the lattice and $\mathbf{k}$ is a wavevector from the first Brillouin zone. A linear combination of Bloch waves from the n'th orbital from each atom is called a Bloch sum [28] for the n'th orbital

$$B_{n\mathbf{k}}(\mathbf{r}) = \frac{1}{\sqrt{rN}}\sum_{j=1}^{N}\sum_{i=1}^{r} e^{i\mathbf{k}(\mathbf{R}_j+\boldsymbol{\tau}_i)}\phi_n(\mathbf{r}-\mathbf{R}_j-\boldsymbol{\tau}_i), \tag{3.1.5}$$

where n is the orbital index, j runs over the N unit cells, i over the atoms in each cell and the prefactor ensures normalization. The motivation behind the name is that it satisfies Bloch's theorem [29]

$$B_{n\mathbf{k}}(\mathbf{r}+\mathbf{R}_j) = e^{i\mathbf{kR}_j}B_{n\mathbf{k}}(\mathbf{r}), \tag{3.1.6}$$

where $\mathbf{R}_j$ is an arbitrary lattice vector. The Bloch sum is not an eigenfunction of the crystal Hamiltonian itself, thus the wave function is obtained as a linear combination of the Bloch sum for different orbitals

$$\psi_{\mathbf{k}}(\mathbf{r}) = \sum_n b_n(\mathbf{k})B_{n\mathbf{k}}(\mathbf{r}), \tag{3.1.7}$$

where the coefficients $b_n(\mathbf{k})$ are constrained to

$$\sum_n |b_n(\mathbf{k})|^2 = 1. \tag{3.1.8}$$

The coefficients $b_n(\mathbf{k})$ will determine the contribution from the Bloch sum of the n'th orbital to the wave function. This wave function satisfies the Schrödinger equation

$$H\psi_{\mathbf{k}}(\mathbf{r}) = \mathcal{E}_{\mathbf{k}}\psi_{\mathbf{k}}(\mathbf{r}), \tag{3.1.9}$$

where the eigenvalues give the electron band structure. To transform the equation into an eigenvalue problem, it is multiplied from left by the Bloch sum $B^*_{m\mathbf{k}'}\delta_{\mathbf{k}\mathbf{k}'} = B^*_{m\mathbf{k}}$ and integrated over the whole space. Note that the Bloch sum at each side of the equation have equal labels $\mathbf{k}$ but different orbital indices. The eigenvalue problem takes the form

$$\sum_n H_{m,n}(\mathbf{k})b_n(\mathbf{k}) = \mathcal{E}_{\mathbf{k}}\sum_n S_{m,n}(\mathbf{k})b_n(\mathbf{k}), \tag{3.1.10}$$

with matrix elements

$$\begin{aligned} H_{m,n}(\mathbf{k}) &= \int \mathrm{d}\mathbf{r}\, B^*_{m\mathbf{k}}(\mathbf{r})\hat{H}B_{n\mathbf{k}}(\mathbf{r}) \\ S_{m,n}(\mathbf{k}) &= \int \mathrm{d}\mathbf{r}\, B^*_{m\mathbf{k}}(\mathbf{r})B_{n\mathbf{k}}(\mathbf{r}). \end{aligned} \tag{3.1.11}$$

The matrix $H(\mathbf{k})$ is the Hamiltonian matrix [2], and S is called the overlap matrix. The eigenvalue problem can be compactly expressed as a matrix equation

$$[H(\mathbf{k}) - \mathcal{E}_{\mathbf{k}}S(\mathbf{k})]\, b_{\mathbf{k}} = 0. \tag{3.1.12}$$

In general $S(\mathbf{k})$ is not equal to identity, hence the matrix equation is a generalized eigenvalue problem, known as a secular equation. By using this approach, the resulting bands will be double degenerate as there is no spin dependency in the model.

As a last remark, note that utilizing the eigenvectors obtained by solving the secular equation, the Hamiltonian can be diagonalized. The corresponding basis is obtained as a linear combination of the old. Thus the diagonal Hamiltonian will describe quasiparticles rather than electrons.

[2] It goes also by the name jumping matrix [28]

3.2 The phonon Hamiltonian

Lattices consisting of atoms or molecules are not as perfect in the real world as they are in theory - they contain impurity as well as atomic motion due to thermal fluctuations. The focus of this section will be on the movement, or more precisely, the fluctuation of the atoms around their equilibrium position. To describe this process, the quantum mechanical concept of phonons is introduced. Their analogue in classical mechanics are normal modes, single-frequency lattice oscillations which forms a basis for the vibrations. The phonon is treated as a quasiparticle as it represents an excited quantized state of an vibrational mode of the lattice.

The concept of quantized lattice vibrations was introduced by Einstein in 1907 [30]. In 1930, the Soviet physicist I. Tamm developed these ideas into a theory regarding quantization of elastic oscillations [31], i.e. a quantized sound field. Inspired by the name photon, the fellow Soviet physicist J. Frenkel came up with the name phonon [32], which comes from Greek and translates to sound or voice.

Phonons are classified according to the characteristic of the lattice vibration. Thus they are divided into two branches, an acoustical and an optical. The ions of the optical branch vibrate anti-symmetrically. As the ions are charged, the anti-symmetric vibration will set up dipole moments that couple to the electromagnetic- or the optic field. The acoustical branch is characterized by symmetric ion vibrations, just as the longitudinal mechanical waves known as sound waves. Keeping this in mind, the names optical and acoustical are easily justified.

The classical Hamiltonian for an ion in a lattice is:

$$\hat{H}_i = \frac{\mathbf{p}_i^2}{2M_i} + \sum_{j \neq i}^{N} V(\mathbf{R}_i - \mathbf{R}_j), \tag{3.2.1}$$

where M_i is the mass of lattice site i, N is the total number of lattice sites and the sum over j runs over all other sites of the lattice. V is a Coulomb

potential stemming from the other ions and $\mathbf{R}_j$ is the position of the ion at lattice site j. The full Hamiltonian is obtained by summing the site Hamiltonians

$$\hat{H} = \sum_{i}^{N} \hat{H}_i. \tag{3.2.2}$$

Solving this problem is in general too hard, as the potential is dependent on all of the dN variables, where d denotes the dimensionality of the system and N the total number of lattice sites. A common approximation is to develop the potential in a Taylor series. Hence it is convenient to express the position of lattice site i as a small fluctuation around its equilibrium position. Let $\mathbf{R}_i = \mathbf{R}_i^0 + \mathbf{u}_i$, where $\mathbf{R}_i^0$ is the equilibrium position of the lattice site and $\mathbf{u}_i$ is the small fluctuation. Further, the fluctuation is decomposed onto the three Cartesian directions, $\mathbf{u}_i = x_i\hat{x} + y_i\hat{y} + z_i\hat{z}$.

Moving on, the potential is Taylor expanded in a harmonic approximation.

$$V(\mathbf{R}_i - \mathbf{R}_j) = V(\mathbf{R}_i^0 - \mathbf{R}_j^0) + \frac{\partial V}{\partial R_{i\mu}}\Big|_{\mathbf{R}=\mathbf{R}_i^0} \Delta R_{i\mu} + \frac{1}{2}\frac{\partial^2 V}{\partial R_{i\mu}\partial R_{j\nu}}\Big|_{\mathbf{R}=\mathbf{R}_i^0} \Delta R_{i\mu}\Delta R_{j\nu}, \tag{3.2.3}$$

where $\{\mu,\nu\} = \{x,y,z\}$ and $\Delta R_{i\mu} = R_{i\mu} - R_{i\mu}^0$. The zeroth order term is a constant and therefore excluded. The first order term involves a first order derivative evaluated at the equilibrium position, which is zero by definition. The lowest order remaining term is the quadratic. Written out explicitly it reads:

$$\begin{aligned} V(\mathbf{R}_i - \mathbf{R}_j)^{(2)} = \frac{1}{2!}\Bigg(& \frac{\partial^2 V}{\partial x_i \partial x_j}\Big|_{\mathbf{R}=\mathbf{R}_i^0} \Delta x_i \Delta x_j + \frac{\partial^2 V}{\partial x_i \partial y_j}\Big|_{\mathbf{R}=\mathbf{R}_i^0} \Delta x_i \Delta y_j + \frac{\partial^2 V}{\partial x_i \partial z_j}\Big|_{\mathbf{R}=\mathbf{R}_i^0} \Delta x_i \Delta z_j \\ & + \frac{\partial^2 V}{\partial y_i \partial x_j}\Big|_{\mathbf{R}=\mathbf{R}_i^0} \Delta y_i \Delta x_j + \frac{\partial^2 V}{\partial y_i \partial y_j}\Big|_{\mathbf{R}=\mathbf{R}_i^0} \Delta y_i \Delta y_j + \frac{\partial^2 V}{\partial y_i \partial z_j}\Big|_{\mathbf{R}=\mathbf{R}_i^0} \Delta y_i \Delta z_j \\ & + \frac{\partial^2 V}{\partial z_i \partial x_j}\Big|_{\mathbf{R}=\mathbf{R}_i^0} \Delta z_i \Delta x_j + \frac{\partial^2 V}{\partial z_i \partial y_j}\Big|_{\mathbf{R}=\mathbf{R}_i^0} \Delta z_i \Delta y_j + \frac{\partial^2 V}{\partial z_i \partial z_j}\Big|_{\mathbf{R}=\mathbf{R}_i^0} \Delta z_i \Delta z_j \Bigg). \end{aligned}$$

Hence, the potential part of the Hamiltonian is

$$\hat{H}^{pot} = \frac{1}{2}\sum_{ij}\sum_{\mu\nu}\Delta R_{i\mu}\Phi^{ij}_{\mu\nu}\Delta R_{j\nu}, \tag{3.2.4}$$

where the force constant matrix $\Phi_{\mu\nu}$ has been defined, with $\{\mu,\nu\} = \{x,y,z\}$. The corresponding matrix elements are

$$\Phi^{ij}_{\mu\nu} = \frac{\partial^2 V}{\partial R_{i\mu}\partial R_{j\nu}}\Big|_{\mathbf{R}=\mathbf{R}^0_i}, \tag{3.2.5}$$

where i and j give the ions involved. Having determined the force constant matrix, one may obtain the equation of motion for ion i, e.g. by calculating the Lagrangian of the system and the associated Lagrange's equation

$$\sum_{i\mu} M_i \Delta\ddot{R}_{i\mu} = -\sum_{ij\mu\nu}\Phi^{ij}_{\mu\nu}\Delta R_{j\nu}, \tag{3.2.6}$$

where the double dots represent the second time derivative of the displacement. To remove the time dependency the displacements are assumed to follow a harmonic oscillation which motivates the ansatz

$$\Delta R_{i\mu} = u_{i\mu}e^{i\omega_{i\mu}t}. \tag{3.2.7}$$

Inserting it into the equation of motion yields

$$\sum_{i\mu} M_i\omega^2_{i\mu}u_{i\mu} = \sum_{ij\mu\nu}\Phi^{ij}_{\mu\nu}u_{j\nu}. \tag{3.2.8}$$

As the lattice is periodical, the position vector $\mathbf{R}_j$ is decomposed into a lattice vector giving the j'th unit cell and a component giving the relative position of the ion within the unit cell, i.e. $\mathbf{R}_j \to \mathbf{R}_j + \boldsymbol{\tau}_i$. Hence the matrix elements of $\Phi_{\mu\nu}$ and the amplitude of the displacement are redefined

$$\Phi^{ij}_{\mu\nu} \to \Phi^{ii'}_{\mu\nu}(j-j') \qquad \text{and} \qquad u_{i\mu} \to u_{ni\mu}, \tag{3.2.9}$$

where j, j' runs over all unit cells and i, i' over the atoms in the unit cell. In addition, the force constants are assumed only dependent on the distance

between the lattice sites and note the sites themselves. The equation of motion takes the form

$$\sum_{ni\mu} M_i \omega_{i\mu}^2 u_{ni\mu} = \sum_{jj'} \sum_{ii'\mu\nu} \Phi_{\mu\nu}^{ii'}(j-j') u_{n'i'\nu}, \tag{3.2.10}$$

where the eigenfrequencies are assumed independent of which unit cell they correspond to. Further, the displacements are Fourier transformed

$$u_{ji\mu} = \sum_{\mathbf{q}} \frac{1}{\sqrt{M_i}} c_{i\mu} e^{i\mathbf{q}(\mathbf{R}_j + \boldsymbol{\tau}_i)}, \tag{3.2.11}$$

where $c_{i\mu}$ is the amplitude. Introducing the vibrations in the equation of motion and solving for ω^2 yields

$$\begin{aligned} \sum_{ji\mu} \omega_{i\mu}^2 c_{i\mu} &= \sum_{jj'} \sum_{ii'\mu\nu} \frac{1}{\sqrt{M_i M_{i'}}} \Phi_{\mu\nu}^{ii'}(j-j') e^{i\mathbf{q}'(\mathbf{R}_{i'} + \boldsymbol{\tau}_{i'})} e^{-i\mathbf{q}(\mathbf{R}_i + \boldsymbol{\tau}_i)} c_{i'\nu} \\ &= \sum_{jj'} \sum_{ii'\mu\nu} \frac{1}{\sqrt{M_i M_{i'}}} \Phi_{\mu\nu}^{ii'}(j-j') e^{i(\mathbf{q}'-\mathbf{q})\mathbf{R}_i} e^{i(\mathbf{q}'(\boldsymbol{\Delta}_{j'j} + \boldsymbol{\tau}_{i'}) - \mathbf{q}\boldsymbol{\tau}_i)} c_{i'\nu}. \end{aligned} \tag{3.2.12}$$

where the lattice vector $\boldsymbol{\Delta}_{j'j} = \mathbf{R}_{j'} - \mathbf{R}_j$. As the force constants are only dependent on distance, summing over j is not an issue, and results in a factor N and $N\delta(\mathbf{q}' - \mathbf{q})$ on respectively, the left- and right-hand side of the equation. Hence the equation of motion becomes

$$\begin{aligned} \sum_{i\mu} \omega_{i\mu}^2 c_{i\mu} &= \sum_{ii'\mu\nu} \left(\sum_{j'} \frac{1}{\sqrt{M_i M_{i'}}} \Phi_{\mu\nu}^{ii'}(j') e^{i\mathbf{q}\mathbf{R}_{j'}^{ii'}} \right) c_{i'\nu} \\ &= \sum_{ii'\mu\nu} D_{\mu\nu}^{ii'}(\mathbf{q}) c_{i'\nu} \end{aligned} \tag{3.2.13}$$

where $\mathbf{R}_{j'}^{ii'} = \boldsymbol{\Delta}_{j'j} + \boldsymbol{\tau}_{i'} - \boldsymbol{\tau}_i$ is the vector linking the atom at relative position i within the unit cell of the centre of the coordinate system to the atom at position i' in the j'th unit cell. In addition, the matrix element $D_{\mu\nu}^{ii'}(\mathbf{q})$ has been introduced:

$$D_{\mu\nu}^{ii'}(\mathbf{q}) = \sum_{j'} \frac{1}{\sqrt{M_i M_{i'}}} \Phi_{\mu\nu}^{ii'}(j') e^{i\mathbf{q}\mathbf{R}_{j'}^{ii'}} \tag{3.2.14}$$

The matrix D is the dynamic matrix and is the Fourier transform of a scaled version of the force constant matrix. By treating the amplitudes, $c_{i\mu}$, as a basis for the vibration, writing the equation in matrix form, multiplying from left by $c^{\dagger}_{i\mu}$, where † denotes the Hermitian conjugate, an eigenvalue problem is obtained

$$\omega^2_{\mathbf{q}} = c^{\dagger} D(\mathbf{q}) c. \tag{3.2.15}$$

Hence it is clear that the eigenvalues of the dynamic matrix give the eigenfrequencies.

The resulting eigenvalue problem of $d \cdot r$ equations is a much simpler problem to solve than the original system of $d \cdot r \cdot N$ equations, where r denotes the number of atoms in the unit cell and d the dimensionality of the system. The cost of the simplification is that the dispersion has to be obtained for each $\mathbf{q}$ in the first Brillouin zone. However, calculating for each $\mathbf{q}$ is a much easier than solving the original system of equations.

3.3 Electron-phonon coupling

Electron-phonon coupling[3] (EPC) is a fundamental interaction in condensed matter systems as it couples the electron and ion subsystems. The interaction is the mechanism behind phonon scattering of electrons, which causes electrical resistance. In addition, the coupling is essential in the description of conventional superconductivity due to a phonon exchange which results in an effective attraction between electrons [33].

The Hamiltonian of a interacting electron system is

$$\hat{H} = \sum_i \frac{\mathbf{p}_i^2}{2m} + \sum_j V(\mathbf{r}_i, \mathbf{R}_j), \tag{3.3.1}$$

[3]The electron-phonon coupling also goes by the name electron-phonon interaction.

where $\mathbf{p}_i$ is the momentum of electron i at position $\mathbf{r}_i$, V is the potential from the lattice and $\mathbf{R}_j$ is the position of the ion at lattice site j. The potential is only dependent on the positions through the distance, meaning $V(\mathbf{r}_i, \mathbf{R}_j) \rightarrow V(\mathbf{r}_i - \mathbf{R}_j)$. It is convenient to decompose the position of the ion as a small fluctuation around its equilibrium position, $\mathbf{R}_j = \mathbf{R}_j^0 + \mathbf{u}_j$, where $\mathbf{R}_j^0$ denotes the equilibrium position for ion j and $\mathbf{u}_j$ is the fluctuation. The potential is then developed in a Taylor series around the equilibrium position

$$V(\mathbf{r}_i - \mathbf{R}_j) = V(\mathbf{r}_i - \mathbf{R}_j^0) + \mathbf{u}_j \nabla_{\mathbf{R}_j} V \Big|_{\mathbf{r}_i - \mathbf{R}_j^0} + \ldots \tag{3.3.2}$$

When the fluctuations are small, a development to first order is assumed to be sufficient for describing weak electron-phonon coupling. The zeroth order term gives the contribution from a static lattice, while the first order term is responsible for the electron-phonon coupling.

By choosing the basis to be Bloch sums in a tight-binding model, as introduced in section 3.1, the Hamiltonian is brought to second quantized form

$$\hat{H} = \hat{H}_0 + \sum_{\mathbf{k}'\mathbf{k}\alpha\beta} \int \mathrm{d}\mathbf{r} \;\; \phi_{\mathbf{k}'}^{\beta\,*}(\mathbf{r}) \mathbf{u}_j \nabla_{\mathbf{R}_j} V(\mathbf{r} - \mathbf{R}_j) \Big|_{\mathbf{r}_i - \mathbf{R}_j^0} \phi_{\mathbf{k}}^{\alpha}(\mathbf{r}) c_{\mathbf{k}'\beta}^{\dagger} c_{\mathbf{k}\alpha}, \tag{3.3.3}$$

where $\hat{H}_0$ is the Hamiltonian of the unperturbed system and the electron states are in the band basis, where the unperturbed Hamiltonian is diagonal. Focus on the part describing the electron-phonon coupling. Note that

$$\nabla_{\mathbf{R}_j} V(\mathbf{r} - \mathbf{R}_j) = -\nabla_{\mathbf{r}} V(\mathbf{r} - \mathbf{R}_j). \tag{3.3.4}$$

Integration by parts is applied to move the differentiation operator from $V(\mathbf{r} - \mathbf{R}_j)$ to $\phi_{\mathbf{k}'}^{\beta\,*}(\mathbf{r})\phi_{\mathbf{k}}^{\alpha}(\mathbf{r})$, which is convenient as the potential $V(\mathbf{r} - \mathbf{R}_j)$ is unknown, while the basis $\phi_{\mathbf{k}}^{\alpha}(\mathbf{r})$ is known

$$\begin{aligned} -\int \mathrm{d}\mathbf{r} \;\; \phi_{\mathbf{k}'}^{\beta\,*}(\mathbf{r}) \phi_{\mathbf{k}}^{\alpha}(\mathbf{r}) \nabla_{\mathbf{r}} V(\mathbf{r} - \mathbf{R}_j) \Big|_{\mathbf{r}_i - \mathbf{R}_j^0} &= -\phi_{\mathbf{k}'}^{\beta\,*}(\mathbf{r}) \phi_{\mathbf{k}}^{\alpha}(\mathbf{r}) V(\mathbf{r} - \mathbf{R}_j^0) \Big|_{\mathbf{r}=-\infty}^{\mathbf{r}=\infty} \\ &\quad + \int \mathrm{d}\mathbf{r} \;\; V(\mathbf{r} - \mathbf{R}_j^0) \nabla_{\mathbf{r}} \left[\phi_{\mathbf{k}'}^{\beta\,*}(\mathbf{r}) \phi_{\mathbf{k}}^{\alpha}(\mathbf{r}) \right]. \end{aligned}$$

The surface term vanishes due to periodical boundary conditions. Note that the factor $V(\mathbf{r}-\mathbf{R}_j^0)$ is present in the expression. Previously it has been stated that $V(\mathbf{r}-\mathbf{R}_j)$ is an unknown quantity, however, it is possible to approximate $V(\mathbf{r}-\mathbf{R}_j^0)$ as it depends on the fixed position $\mathbf{R}_j^0$, rather than the unknown $\mathbf{R}_j$. The derivation term is written out explicitly as

$$\begin{aligned}\nabla_{\mathbf{r}}\left[\phi^{\beta\,*}_{\mathbf{k}'}(\mathbf{r})\phi^{\alpha}_{\mathbf{k}}(\mathbf{r})\right] &= \nabla_{\mathbf{r}}\left[e^{i(\mathbf{k}-\mathbf{k}')\mathbf{r}}u^{\beta\,*}_{\mathbf{k}'}(\mathbf{r})u^{\alpha}_{\mathbf{k}}(\mathbf{r})\right]\\ &= -i\mathbf{q}e^{-i\mathbf{q}\mathbf{r}}u^{\beta\,*}_{\mathbf{k}+\mathbf{q}}(\mathbf{r})u^{\alpha}_{\mathbf{k}}(\mathbf{r})\\ &\quad + e^{-i\mathbf{q}\mathbf{r}}\left(u^{\beta\,*}_{\mathbf{k}+\mathbf{q}}(\mathbf{r})\nabla_{\mathbf{r}}u^{\alpha}_{\mathbf{k}}(\mathbf{r}) + u^{\alpha}_{\mathbf{k}}(\mathbf{r})\nabla_{\mathbf{r}}u^{\beta\,*}_{\mathbf{k}+\mathbf{q}}(\mathbf{r})\right),\end{aligned} \tag{3.3.5}$$

where $\mathbf{q}=\mathbf{k}'-\mathbf{k}$ has been introduced. The expression obtained using integration by parts is a vector quantity and is compactly defined as

$$\mathbf{W}^{\alpha\beta}_{\mathbf{k}\mathbf{q}} \equiv \int \mathrm{d}\mathbf{r}\left(-i\mathbf{q}u^{\beta\,*}_{\mathbf{k}+\mathbf{q}}(\mathbf{r})u^{\alpha}_{\mathbf{k}}(\mathbf{r}) + \left(u^{\beta\,*}_{\mathbf{k}+\mathbf{q}}(\mathbf{r})\nabla_{\mathbf{r}}u^{\alpha}_{\mathbf{k}}(\mathbf{r}) + u^{\alpha}_{\mathbf{k}}(\mathbf{r})\nabla_{\mathbf{r}}u^{\beta\,*}_{\mathbf{k}+\mathbf{q}}(\mathbf{r})\right)e^{-i\mathbf{q}\mathbf{r}}V(\mathbf{r}-\mathbf{R}_i^0)\right) \tag{3.3.6}$$

where the integral goes over the whole space. Hence the Hamiltonian takes the form

$$H_{\mathrm{el-ph}} = \sum_j \sum_{\mathbf{k}\mathbf{q}\alpha\beta} \mathbf{u}_j \mathbf{W}^{\alpha\beta}_{\mathbf{k}\mathbf{q}} c^{\dagger}_{\mathbf{k}+\mathbf{q},\beta} c_{\mathbf{k}\alpha}. \tag{3.3.7}$$

To obtain a second quantized Hamiltonian, the displacement or fluctuation $\mathbf{u}_j$ is brought to second quantized form. As presented in section 3.2, the quantized version of lattice fluctuations are phonons. In second quantization they have the form [34]

$$\sum_j \mathbf{u}_j = \sum_{\mathbf{q}\lambda} \frac{1}{\sqrt{2NM\omega_{\mathbf{q}\lambda}}}\mathbf{e}_{\lambda}(\mathbf{q})\left(a_{\mathbf{q}\lambda} + a^{\dagger}_{-\mathbf{q}\lambda}\right), \tag{3.3.8}$$

where M is the mass of the ion, N is the number of lattice sites, $\mathbf{e}_{\lambda}(\mathbf{q})$ is a vector giving the direction of the vibration, and $\omega_{\mathbf{q}\lambda}$ is the eigenfrequency of vibrational mode λ at $\mathbf{q}$. Note that the operators $a_{\mathbf{q}\lambda}$ and $a^{\dagger}_{-\mathbf{q}\lambda}$ are in

the diagonal basis of the phonon Hamiltonian. Thus the electron-phonon coupling can be expressed compactly

$$H_{\text{el-ph}} = \sum_{\mathbf{kq}} \sum_{\alpha\beta\lambda} g^{\alpha\beta\lambda}_{\mathbf{k},\mathbf{k+q}} c^{\dagger}_{\mathbf{k+q}\beta} c_{\mathbf{k}\alpha} \left(a_{\mathbf{q}\lambda} + a^{\dagger}_{-\mathbf{q}\lambda} \right), \tag{3.3.9}$$

where the electron-phonon coupling constant has been introduced

$$g^{\alpha\beta\lambda}_{\mathbf{k},\mathbf{k+q}} = \frac{\mathbf{W}^{\alpha\beta}_{\mathbf{k},\mathbf{k+q}} \cdot \mathbf{e}_{\lambda}(\mathbf{q})}{\sqrt{2NM\omega_{\mathbf{q}\lambda}}}. \tag{3.3.10}$$

The electron-phonon coupling corresponds to the scattering process visualized in Figure 3.3.1.

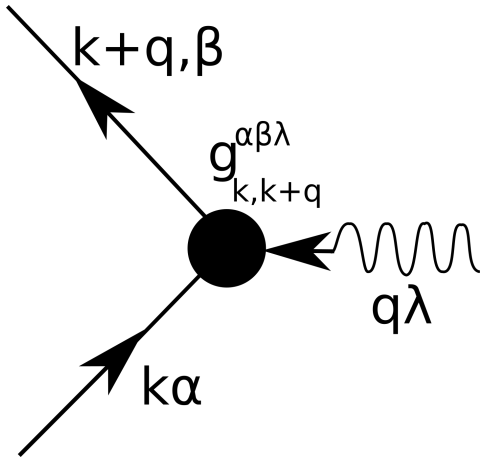

Figure 3.3.1: The scattering process where an incident quasiparticle in state $(\mathbf{k}\alpha)$ interacts with a phonon in state $(\mathbf{q}\lambda)$ and is scattered into the outgoing state $(\mathbf{k}+\mathbf{q},\beta)$ is visualized in the figure. The vertex represents $g^{\alpha\beta\lambda}_{\mathbf{k},\mathbf{k+q}}$, the probability amplitude of the scattering process.

The physical interpretation of the coupling constant $g^{\alpha\beta\lambda}_{\mathbf{k},\mathbf{k+q}}$ is the probability of the inelastic scattering process where an incident quasiparticle in state

($\mathbf{k}\alpha$), assisted by the creation (annihilation) of a phonon in state $a^{\dagger}_{-\mathbf{q}\lambda}(a_{\mathbf{q}\lambda})$, is scattered into the outgoing state $(\mathbf{k}+\mathbf{q},\beta)$ [35], where $\{\alpha,\beta\}$ are band indices running over the electron bands.

Chapter 4

The bonds in graphene

As previously stated, graphene is a honeycomb lattice of carbon atoms. The aim of this section is to understand why a two-dimensional sheet of carbon atoms has the form of a honeycomb lattice. Section 4.1 provides an introduction to a general honeycomb lattice, where symmetries and relevant quantities are emphasized. In section 4.2, the atomic orbitals are related to the bonds of graphene.

4.1 The honeycomb lattice

The honeycomb lattice is visualized in Figure 4.1.1, and is a triangular lattice with a two-atomic basis, or equivalently, two interpenetrating triangular lattices shifted $a\hat{y}$ relative to one another. It is spanned by the lattice vectors $\mathbf{a}_1 = \sqrt{3}a$ and $\mathbf{a}_2 = \frac{\sqrt{3}}{2}a\hat{x} + \frac{3}{2}a\hat{y}$, where a is the lattice constant. The lattice vectors coincide with $\boldsymbol{\gamma}_1$ and $\boldsymbol{\gamma}_3$ in the figure.

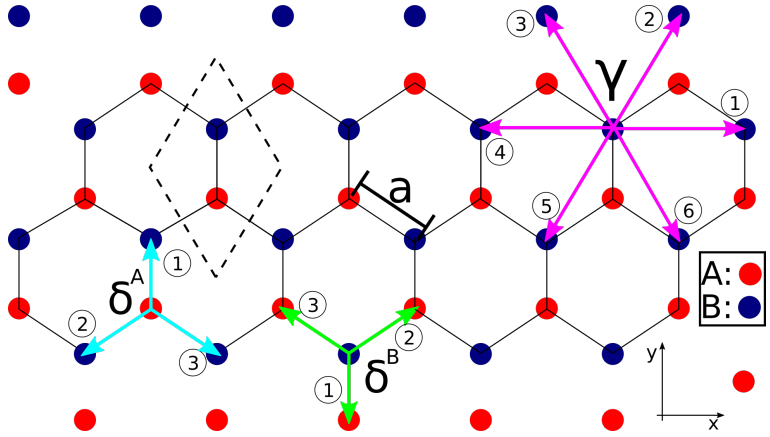

Figure 4.1.1: The unit cell is visualized as the dashed parallelogram and consists of a two-atomic basis where an atom of type A is located at $(0,-a/2)$ and an atom of type B at $(0,a/2)$. The lattice constant a is the distance between an atom and its nearest neighbour. The delta vectors, $\boldsymbol{\delta}_j^{(A,B)}$, show the relative position of the nearest neighbours of an atom of type A or B. The gamma vector, $\boldsymbol{\gamma}$, shows the relative position of the next nearest neighbours or equivalently, the nearest neighbours on the same sublattice, and is equal for both types of lattice sites.

The lattice exhibits mirror symmetry about the x-axis dividing any unit cell in two mirror-symmetric parts. Thus the atoms of the unit cell, labelled A and B respectively, experience the lattice differently. The relative position of the nearest neighbours (NN) is denoted $\boldsymbol{\delta}_i^{A(B)}$, where $i = 1,2,3$.

$$\begin{aligned} \boldsymbol{\delta}_1^A &= a\hat{y} & \boldsymbol{\delta}_1^B &= -a\hat{y} \\ \boldsymbol{\delta}_2^A &= -\frac{a}{2}(\sqrt{3}\hat{x}+\hat{y}) & \boldsymbol{\delta}_2^B &= \frac{a}{2}(\sqrt{3}\hat{x}+\hat{y}) \\ \boldsymbol{\delta}_3^A &= \frac{a}{2}(\sqrt{3}\hat{x}-\hat{y}) & \boldsymbol{\delta}_3^B &= \frac{a}{2}(-\sqrt{3}\hat{x}+\hat{y}) \end{aligned} \tag{4.1.1}$$

The next nearest neighbours (NNN) of any lattice site equal the NN of the

same sublattice. Their relative position is denoted $\boldsymbol{\gamma}_i$:

$$\begin{aligned} \boldsymbol{\gamma}_1 &= \sqrt{3}a\hat{x} & \boldsymbol{\gamma}_4 &= -\sqrt{3}a\hat{x} \\ \boldsymbol{\gamma}_2 &= a\left(\frac{\sqrt{3}}{2}\hat{x} + \frac{3}{2}\hat{y}\right) & \boldsymbol{\gamma}_5 &= -a\left(\frac{\sqrt{3}}{2}\hat{x} + \frac{3}{2}\hat{y}\right). \\ \boldsymbol{\gamma}_3 &= a\left(-\frac{\sqrt{3}}{2}\hat{x} + \frac{3}{2}\hat{y}\right) & \boldsymbol{\gamma}_6 &= a\left(\frac{\sqrt{3}}{2}\hat{x} - \frac{3}{2}\hat{y}\right) \end{aligned} \tag{4.1.2}$$

The reciprocal lattice, as visualized in Figure 4.1.2, is itself a honeycomb lattice, but rotated $\pi/6$ relative to the real-space lattice. It is spanned by the reciprocal lattice vectors $\mathbf{b}_1 = \frac{2\pi}{3a}\left(\sqrt{3}\hat{x} - \hat{y}\right)$ and $\mathbf{b}_2 = \frac{4\pi}{3a}\hat{y}$. The first Brillouin zone is marked as the green hexagon and is given as a Wigner-Seitz cell [27]. The high-symmetry points are marked according to their position.

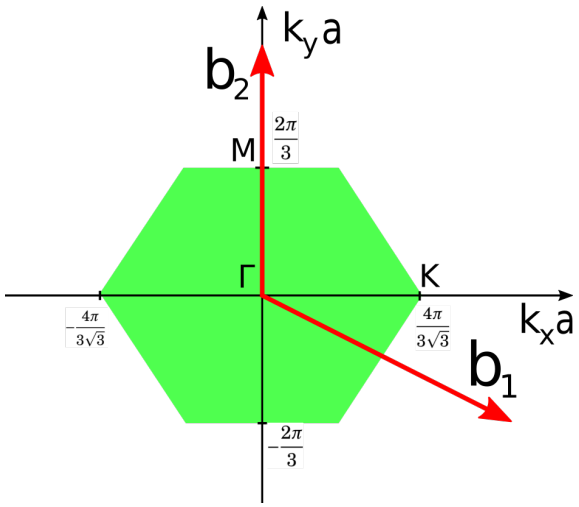

Figure 4.1.2: The reciprocal lattice vectors b_1 and b_2 are plotted against the dimensionless variable $\mathbf{k}a$. The green hexagon shows the first Brillouin zone and the high symmetry points are marked according to their position.

4.2 Linking the atomic orbitals to the bonds in graphene

The carbon atom has four valence electrons and can thus form up to four bonds. As graphene is a result of sp^2 hybridization, three of the electrons are used for creating σ bonds, while the remaining electron forms a π bond [36]. The σ bonds lies in the same plane, defined as the xy-plane, and are oriented $2\pi/3$ relative to one another. The exceptional mechanical properties, introduced in section 1.1 are due to them, and thus they are often dubbed as strong σ bonds. The π bond is oriented orthogonal to the plane, i.e. in the z direction, and is responsible for the formidable electron transport properties [12]. In addition, π bonds from different sheets of graphene interact through van der Waals forces binding the sheets together and thereby forming graphite [36]. In this context, the (out-of-plane) bonds of graphene are soft, which is why graphite is useful in pencils.

The bonds are formed by linear combinations of the eigenfunctions of the Hydrogen atom, ψ_{nlm}, where n is known as the principal quantum number, l the orbital quantum number and m the magnetic quantum number. They are well known functions of generalized Laguerre polynomials and spherical harmonic functions, and the first five, corresponding to quantum numbers $n = 1$ and $n = 2$ are [37]

$$\begin{aligned}
\psi_{100}(\mathbf{r}) &= \frac{1}{\sqrt{\pi r_B^3}} e^{-\frac{r}{r_B}} & \psi_{211}(\mathbf{r}) &= \frac{1}{\sqrt{64\pi r_B^5}} r\sin(\theta) e^{i\phi} e^{-\frac{r}{2r_B}} \\
\psi_{200}(\mathbf{r}) &= \frac{1}{\sqrt{32\pi r_B^3}} \left(2 - \frac{r}{r_B}\right) e^{-\frac{r}{2r_B}} & \psi_{21-1}(\mathbf{r}) &= \frac{1}{\sqrt{64\pi r_B^5}} r\sin(\theta) e^{-i\phi} e^{-\frac{r}{2r_B}}, \\
\psi_{210}(\mathbf{r}) &= \frac{1}{\sqrt{32\pi r_B^5}} r\cos(\theta) e^{-\frac{r}{2r_B}}
\end{aligned} \tag{4.2.1}$$

where r_B denotes the Bohr radius and $\mathbf{r} = (r, \phi, \theta)$ is the position expressed

in spherical coordinates. The corresponding atomic orbitals are [38]

$$\begin{aligned} |1s\rangle &= \psi_{100} & |2p_x\rangle &= \frac{1}{\sqrt{2}}\left(\psi_{21-1} + \psi_{211}\right) \\ |2s\rangle &= \psi_{200} & \left|2p_y\right\rangle &= \frac{i}{\sqrt{2}}\left(\psi_{21-1} - \psi_{211}\right), \\ |2p_z\rangle &= \psi_{210} \end{aligned} \tag{4.2.2}$$

where the s orbitals are symmetric, while the p orbitals are anti-symmetric. Note that the orbitals $|2p_x\rangle$ and $\left|2p_y\right\rangle$ are formed by linear combinations of the eigenstates to ensure an anti-symmetric form. The π bond corresponds to the $|2p_z\rangle$ orbital, while the three σ bonds are formed by linear combinations of the eigenstates [39]. Hence the four orbitals of each atom are:

$$\begin{aligned} &|2p_z\rangle & &\left|sp_2^2\right\rangle = \frac{1}{\sqrt{3}}\left(|2s\rangle - \frac{1}{\sqrt{2}}\left|2p_y\right\rangle - \sqrt{\frac{3}{2}}\,|2p_x\rangle\right) \\ &\left|sp_1^2\right\rangle = \frac{1}{\sqrt{3}}\left(|2s\rangle - \sqrt{2}\left|2p_y\right\rangle\right) & &\left|sp_3^2\right\rangle = \frac{1}{\sqrt{3}}\left(|2s\rangle - \frac{1}{\sqrt{2}}\left|2p_y\right\rangle + \sqrt{\frac{3}{2}}\,|2p_x\rangle\right) \end{aligned}$$

For the carbon atoms to form σ bonds, the atomic orbitals associated with the sp^2 hybridization must overlap with sp^2-orbitals from other atoms. The most stable situation, i.e. the strongest bond, is obtained by maximizing the overlap of the orbitals, which is done by orienting them along the same line. As the sp^2-orbitals exhibit three-fold symmetry, the atoms at each end of a σ bond must be mirror images of one another. Hence a crystal formed by atoms exhibiting sp^2 hybridization results in a honeycomb lattice, as shown in Figure 4.1.1. As a consequence, the atomic orbitals must be labelled $A(B)$ to indicate their orientation

$$
\begin{aligned}
&\left|2p_z^{A(B)}\right\rangle \\
&\left|\left(sp_1^2\right)^{A(B)}\right\rangle = \frac{1}{\sqrt{3}}\left(|2s\rangle \mp \sqrt{2}\left|2p_y\right\rangle\right) \\
&\left|\left(sp_2^2\right)^{A(B)}\right\rangle = \frac{1}{\sqrt{3}}\left(|2s\rangle \pm \frac{1}{\sqrt{2}}\left|2p_y\right\rangle \pm \sqrt{\frac{3}{2}}|2p_x\rangle\right) \\
&\left|\left(sp_3^2\right)^{A(B)}\right\rangle = \frac{1}{\sqrt{3}}\left(|2s\rangle \pm \frac{1}{\sqrt{2}}\left|2p_y\right\rangle \mp \sqrt{\frac{3}{2}}|2p_x\rangle\right),
\end{aligned}
\tag{4.2.3}
$$

where the upper signs are for orbitals at lattice site A and the lower for lattice site B.

An alternative notation for an orbital is $\phi_{r_B}^o(\mathbf{r})^{A(B)} = \left\langle \mathbf{r}\middle| o^{A(B)}\right\rangle$, where o is the orbital index and r_B denotes the Bohr radius. The Bohr radius is to be interpreted as the most probable distance from an electron to the nucleus of a Hydrogen atom in its ground state, $\langle 1s|\, r\, |1s\rangle = r_B$. Hence it is a measure of the width of the orbitals and thus controls the overlap of orbitals from the different atoms.

When modelling graphene, it is crucial to pick a Bohr radius that gives orbital overlaps that resemble the physical situation in graphene. A measure of the overlap is the electron density, which is plotted for three values of the Bohr radius in Figure 4.2.1. As the figure shows, picking r_B too small results in no overlap at all as the electrons are too tightly bound to the nucleus. Picking it too large results in a strong bond between the two atoms of the unit cell, but weak bonds between atoms of different unit cells. A suitable value for the Bohr radius is $r_B = a/10$, as it results in a bond that both links the two atoms in the unit cell, as well as atoms across unit cell boundaries.

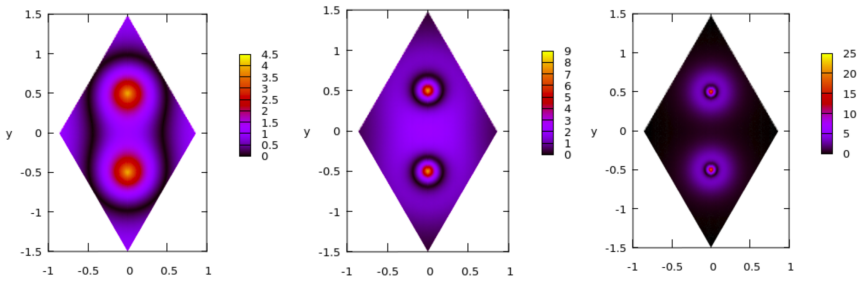

(a) $r_B = a/3$ **(b)** $r_B = a/10$ **(c)** $r_B = a/25$

Figure 4.2.1: The electron density is plotted over the unit cell for $z = 0$ for different values of r_B.

Chapter 5

Results

In this section, the models introduced in section 3 are specialized to graphene. For each of the models, an explicit expression is derived.

In section 5.1, the secular equation (3.1.12) is adapted to graphene and the band structure is obtained. Section 5.2 contains a specialization of the dynamic matrix to graphene and the derivation of an analytic expression for the phonon dispersion and its corresponding eigenvalues. Finally, in section 5.3, the electron-phonon coupling constant is adapted to the low temperature limit and its dependency on the Fermi energy is investigated.

5.1 The band structure

The band structure are given as the eigenvalues of the electron system, determined by the generalized eigenvalue problem given by the secular equation (3.1.12). By solving the equation, the electron bonds of graphene are linked to the bands. As pointed out in section 3.1, the bonds are due to electrons, while the band structure is linked to quasiparticles, given by linear combinations of the atomic orbitals. Hence the band structure yields the

allowed energies for a given band and momentum.

In section 5.1.1, the matrix elements of the secular equation are derived. Some additional theory on decomposition of p orbitals in components parallel and orthogonal to the direction of the bond, is presented in section 5.1.1.1. In sections 5.1.2 and 5.1.3 explicit expressions for the matrix elements associated with, respectively the π and σ bands are found. Finally, in section 5.1.4, the band structure is plotted.

5.1.1 Adapting the secular equation to graphene

As introduced in section 4.2, linear combinations of the $2s$, $2p_x$ and $2p_y$ orbitals form three σ bonds while the $2p_z$ orbital single-handedly forms a π bond. To obtain the band structure of graphene, the tight-binding model introduced in section 3.1 is used, under the assumption that the overlap of orbitals is non-zero only for nearest neighbours.

To solve the secular equation (3.1.12), the matrix elements involved need to be calculated. In addition, a well-defined basis is needed to state the generalized eigenvalue problem properly. Here the ordering

$$\begin{bmatrix} 2s^A & 2p_x^A & 2p_y^A & 2s^B & 2p_x^B & 2p_y^B & 2p_z^A & 2p_z^B \end{bmatrix}^T \tag{5.1.1}$$

will be used. As the $2p_z$ orbital only contribute the π bond, the matrices of the generalized eigenvalue problem will be Bloch diagonal, factorized in a 6×6 and a 2×2 matrix. Their respective eigenvalues will give the six bands associated with the σ bonds (three from bonding and three from anti-bonding) and the two bands from the π bond and anti-bond [16, 40]. The bands associated with anti-bonds are denoted by an asterisk *, i.e. σ_i^*, where $i = 1,2,3$, and π^*. The π and π^* bands are of special importance as they form the valence and conduction band, respectively, and thus are responsible for the magnificent electronic properties of graphene [12].

The matrix elements, given by equation (3.1.11), are expectation values taken in two Bloch sum states. Next these matrix elements are investigated, starting with the elements of the Hamiltonian matrix

$$
\begin{aligned}
H_{m,i';n,i}(\mathbf{k}) &= \left(\frac{1}{\sqrt{N}}\right)^2 \sum_{j,j'} e^{i\mathbf{k}(\mathbf{R}_j+\boldsymbol{\tau}_i)} e^{-i\mathbf{k}'(\mathbf{R}_{j'}+\boldsymbol{\tau}_{i'})} \int \mathrm{d}\mathbf{r}\ \phi_m^*(\mathbf{r}-\mathbf{R}_{j'}-\boldsymbol{\tau}_{i'})\hat{H}\phi_n(\mathbf{r}-\mathbf{R}_j-\boldsymbol{\tau}_i) \\
&= \frac{1}{N}\sum_{j,j'} e^{i\mathbf{k}((\mathbf{R}_{j'}+\boldsymbol{\Delta}_{j'j})+\boldsymbol{\tau}_i)} e^{-i\mathbf{k}'(\mathbf{R}_{j'}+\boldsymbol{\tau}_{i'})} \\
&\times \int \mathrm{d}\mathbf{r}'\ \phi_m^*(\mathbf{r}')\hat{H}\phi_n(\mathbf{r}'+\mathbf{R}_{j'}+\boldsymbol{\tau}_{i'}-(\mathbf{R}_{j'}+\boldsymbol{\Delta}_{j'j})-\boldsymbol{\tau}_i) \\
&= \frac{1}{N}\sum_{j,j'} e^{i(\mathbf{k}-\mathbf{k}')\mathbf{R}_{j'}} e^{i(\mathbf{k}(\boldsymbol{\Delta}_{j'j}+\boldsymbol{\tau}_i)-\mathbf{k}'\boldsymbol{\tau}_{i'})} \int \mathrm{d}\mathbf{r}'\ \phi_m^*(\mathbf{r}')\hat{H}\phi_n(\mathbf{r}'-\boldsymbol{\delta}_{j'j}^{i'i}) \\
&= \frac{1}{N}\sum_{j,j'} e^{i(\mathbf{k}-\mathbf{k}')\mathbf{R}_{j'}} e^{i(\mathbf{k}(\boldsymbol{\Delta}_{j'j}+\boldsymbol{\tau}_i)-\mathbf{k}'\boldsymbol{\tau}_{i'})} H_{mn}(\boldsymbol{\delta}_{j'j}^{i'i}),
\end{aligned}
\tag{5.1.2}
$$

where $\boldsymbol{\Delta}_{j'j}$ is a lattice vector linking unit cell j' to unit cell j, $\boldsymbol{\delta}_{j'j}^{i'i} = \boldsymbol{\Delta}_{j'j}+\boldsymbol{\tau}_i-\boldsymbol{\tau}_{i'}$, the indices j,j' runs over all lattice sites and the integral is taken over the whole space. The element $H_{mn}(\boldsymbol{\delta}_{jj'}^{i'i})$ is an energy associated with the overlap of orbital m at lattice site i' of unit cell j and orbital n from lattice site i in unit cell j. The vector $\boldsymbol{\delta}_{jj'}^{i'i}$ links these two sites. Furthermore, the elements are independent of the details of the lattice sites and only dependent on the distance, $H_{mn}(\boldsymbol{\delta}_{j'j}^{i'i}) \to H_{mn}(|\boldsymbol{\delta}_{j'j}^{i'i}|)$. Hence, performing the sum over j' results in a δ-function, $\delta_{\mathbf{kk}'}$, and N identical contributions, thus cancelling the $1/N$ prefactor. Thus one obtains

$$
H_{m,i';n,i}(\mathbf{k}) = \sum_j e^{i\mathbf{k}\boldsymbol{\delta}_j^{i'i}} H_{mn}(\boldsymbol{\delta}_j^{i'i}),
\tag{5.1.3}
$$

where $\boldsymbol{\delta}_{j'j}^{i'i} \to \boldsymbol{\delta}_j^{i'i}$, i.e. everything is calculated relative to the unit cell in the centre of the coordinate system.

A similar equation can be obtained for $S_{m,i';n,i}(\mathbf{k})$ by considering the overlap of orbitals instead of the expectation value for the energy in the first line of equation (5.1.2). The resulting matrix elements are

$$
S_{m,i';n,i}(\mathbf{k}) = \sum_j e^{i\mathbf{k}\boldsymbol{\delta}_j^{i'i}} S_{mn}(\boldsymbol{\delta}_j^{i'i}),
\tag{5.1.4}
$$

where the expectation values are

$$H_{m,n}(\boldsymbol{\delta}_j^{i'i}) = \int \mathrm{d}\mathbf{r}\ \phi_m^*(\mathbf{r})\hat{H}\phi_n(\mathbf{r}-\boldsymbol{\delta}_j^{i'i})$$
$$S_{m,n}(\boldsymbol{\delta}_j^{i'i}) = \int \mathrm{d}\mathbf{r}\ \phi_m^*(\mathbf{r})\phi_n(\mathbf{r}-\boldsymbol{\delta}_j^{i'i}), \tag{5.1.5}$$

and non-zero only in the case when lattice site i' of the unit cell defining the origin of the coordinate system and i in unit cell j are NN or is the same lattice point.

5.1.1.1 Decomposition of p orbitals

Before calculating the matrix elements explicitly, expectation values involving p orbitals are investigated. Consider two orbitals residing on two different atoms, where one orbital is specified to be a p orbital while the other is undefined. Let $\mathbf{d}$ be a unit vector in the direction of the bond between the atoms and $\mathbf{n}$ denote a unit vector normal to $\mathbf{d}$. Furthermore, let $\mathbf{a}$ lie in the same plane as $\mathbf{d}$ and be a unit vector in one of the Cartesian directions, i.e. oriented parallel to a p orbital. The situation is shown in Figure 5.1.1.

The p orbital can then be decomposed in two components, one parallel to the bond, $|p_d\rangle$, and one perpendicular to it, $|p_n\rangle$ [40]

$$|p_a\rangle = \mathbf{a}\cdot\mathbf{d}\,|p_d\rangle + \mathbf{a}\cdot\mathbf{n}\,|p_n\rangle = \cos(\theta)\,|p_d\rangle + \sin(\theta)\,|p_n\rangle\,, \tag{5.1.6}$$

where $a = \{x, y, z\}$ and θ is the angle between the Cartesian axis and the direction of the bond. The expectation value between the p orbital and an s orbital becomes

$$\langle s|H|p_a\rangle = \langle s|H|p_d\rangle\cos(\theta) + \langle s|H|p_n\rangle\sin(\theta) = H_{sp\sigma}\cos(\theta), \tag{5.1.7}$$

as $\langle s|H|p_n\rangle$ vanishes due to symmetry (s is even while p_n is odd) and the constant $H_{sp\sigma} = \langle s|H|p_d\rangle$ has been introduced. It is labelled $sp\sigma$ as it is

calculated using an s orbital and a p orbital, while σ indicates that it originates from the effective component parallel to the bond. Matrix elements that originate from the effective normal component to the direction of the bond are labelled π. As interchanging the orbitals in the expectation value is equivalent to reverting the direction of the bond, the Hermitian conjugate, $\langle p_a|H|s\rangle$, is obtained by reverting the direction of the bond, $\mathbf{d} \to -\mathbf{d}$, making $\theta \to \pi - \theta$ which transform $\cos(\pi - \theta) = -\cos(\theta)$. Hence $\langle p_n|H|s\rangle = -\langle s|H|p_n\rangle$.

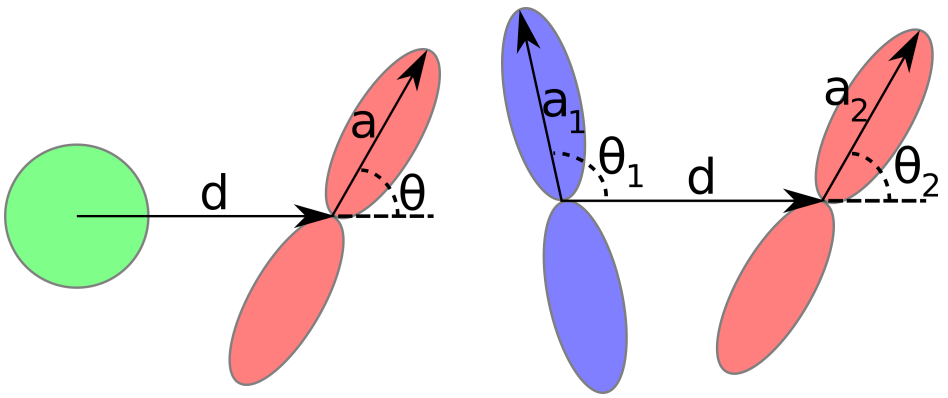

(a) Binding between an s and a p orbital.

(b) Binding between two p orbitals, where both orbitals lie in the same plane.

Figure 5.1.1: A sketch of the binding between a p and a p or s orbtial. The vector $\mathbf{d}$ is a unit vector in the direction of the bond, while the orientation of the p orbital is given by the unit vector $\mathbf{a}$. θ is the angle between the orientation of the p orbital and the direction of the bond.

The matrix element between two p orbitals is also of interest

$$\begin{aligned}\langle p_1|H|p_2\rangle &= \big(\mathbf{a_1}\cdot\mathbf{d}\,\langle p_d| + \mathbf{a_1}\cdot\mathbf{n}\,\langle p_n|\big)H\big(\mathbf{a_2}\cdot\mathbf{d}\,|p_d\rangle + \mathbf{a_2}\cdot\mathbf{n}\,|p_n\rangle\big)\\ &= H_{pp\sigma}\cos(\theta_1)\cos(\theta_2) + H_{pp\pi}\sin(\theta_1)\sin(\theta_2),\end{aligned} \tag{5.1.8}$$

where the cross terms vanish due to orthogonality and $H_{pp\sigma(\pi)}$ is the value of the matrix element between the two effective p orbitals parallel (orthogonal) to the bond direction. The Hermitian conjugate $\langle p_2|H|p_1\rangle$ is obtained by $\mathbf{d} \to -\mathbf{d}$, making $\theta \to \pi - \theta$ which transform the trigonometric functions according to $\sin(\pi-\theta) = \sin(\theta)$ and $\cos(\pi-\theta) = -\cos(\theta)$. As one sees, the net change is identity, hence $\langle p_2|H|p_1\rangle = \langle p_1|H|p_2\rangle$.

The matrix elements associated with the overlap matrix S are obtained analogously, by considering the overlap of the orbitals instead of the expectation values of the Hamiltonian. Summarized briefly, the results are

$$\begin{aligned} \langle s|p_a\rangle &= S_{sp\sigma}\cos(\theta) \\ \langle p_1|p_2\rangle &= S_{pp\sigma}\cos(\theta_1)\cos(\theta_2) + S_{pp\pi}\sin(\theta_1)\sin(\theta_2), \end{aligned} \tag{5.1.9}$$

where the Hermitian conjugates have the same structure as previously, $\langle p_a|s\rangle = -\langle s|p_a\rangle$ and $\langle p_2|p_1\rangle = \langle p_1|p_2\rangle$. As a last remark, note that the relations (5.1.6)-(5.1.9) are derived for orbitals located on different lattice sites under the restriction that the sites are nearest neighbours. The results would have been different if the orbitals were to reside on the same atom, as the orbitals of an atom form an orthonormal basis.

5.1.2 Calculation of π bands

The π and π^* bonds are only made up of the $2p_z$ orbital. As discussed in section 5.1.1, a convenient basis is $\begin{bmatrix} 2p_z^A & 2p_z^B \end{bmatrix}^T$, which gives the Hamiltonian and overlap matrices

$$H = \begin{bmatrix} h^{AA} & h^{AB} \\ h^{BA} & h^{BB} \end{bmatrix} \qquad \text{and} \qquad S = \begin{bmatrix} s^{AA} & s^{AB} \\ s^{BA} & s^{BB} \end{bmatrix}, \tag{5.1.10}$$

where the matrix elements are given by equations (5.1.3) and (5.1.4). As none of the NN of either sublattices belong to the same lattice, the diagonal elements will only depend on overlap of on-site orbitals, while the off-diagonal elements will only depend on overlap of orbitals from NN lattice

sites. Utilizing equation (5.1.3), the sum over j has only one contribution for the diagonal elements, namely when $\boldsymbol{\delta}_j^{i'i} = \boldsymbol{\delta}_{j=0}^{AA(BB)} = 0$. Hence the diagonal entries are simply the expectation value of the Hamiltonian taken in the $2p_z$ orbital of the respective lattice site

$$\begin{aligned} h^{AA} &= \mathcal{E}_{2p_z} \\ h^{BB} &= \mathcal{E}_{2p_z}. \end{aligned} \tag{5.1.11}$$

To derive the off-diagonal elements, the relation for the expectation value of two p orbitals is utilized, given by equation (5.1.8), which requires defining the orientation of the two p orbitals. As the two orbitals are $2p_z$ orbitals, $\mathbf{a}_1 = \mathbf{a}_2 = \hat{z}$. Due to the two-dimensional structure of graphene, the bond between the two atoms lies in the xy-plane, thus only the component normal to the direction of the bond remains. Hence the elements become

$$\begin{aligned} h^{AB} &= \sum_j e^{i\mathbf{k}\boldsymbol{\delta}_j^{AB}} H_{2p_z^A,2p_z^B}(\boldsymbol{\delta}_j^{AB}) = H_{pp\pi} e^{ik_y} \left(1 + 2e^{-i\frac{3}{2}k_y} \cos\left(\frac{\sqrt{3}}{2}k_x\right)\right) \\ h^{BA} &= \sum_j e^{i\mathbf{k}\boldsymbol{\delta}_j^{BA}} H_{2p_z^B,2p_z^A}(\boldsymbol{\delta}_j^{BA}) = \left(h^{AB}\right)^* \end{aligned} \tag{5.1.12}$$

The overlap matrix is obtained in an analogous way. The diagonal elements are identity, which is easily seen from equation (5.1.5) by setting $\boldsymbol{\delta} = 0$ and using that the orbitals are normalized. The off-diagonal elements are

$$\begin{aligned} s^{AB} &= \sum_j e^{i\mathbf{k}\boldsymbol{\delta}_j^{AB}} S_{2p_z^A,2p_z^B}(\boldsymbol{\delta}_j^{AB}) = S_{pp\pi} e^{ik_y} \left(1 + 2e^{-i\frac{3}{2}k_y} \cos\left(\frac{\sqrt{3}}{2}k_x\right)\right) \\ s^{BA} &= \sum_j e^{i\mathbf{k}\boldsymbol{\delta}_j^{BA}} S_{2p_z^B,2p_z^A}(\boldsymbol{\delta}_j^{BA}) = \left(s^{AB}\right)^*. \end{aligned} \tag{5.1.13}$$

5.1.3 Calculation of σ bands

Using the basis introduced in section 5.1.1,

$$\begin{bmatrix} 2s^A & 2p_x^A & 2p_y^A & 2s^B & 2p_x^B & 2p_y^B \end{bmatrix}^T,$$

the Hamiltonian and overlap matrices factorize into 3×3 submatrices

$$H = \begin{bmatrix} H^{AA} & H^{AB} \\ H^{BA} & H^{BB} \end{bmatrix} \qquad \text{and} \qquad S = \begin{bmatrix} S^{AA} & S^{AB} \\ S^{BA} & S^{BB} \end{bmatrix}. \tag{5.1.14}$$

As only NN overlap is assumed non-zero, the elements associated with equal superscript are only dependent on orbitals residing on the same lattice site. Hence the submatrices on the diagonals will themselves be diagonal 3×3 matrices as the orbitals at each site form an orthonormal set, as seen from equation (5.1.5):

$$h_{mn}^{AA(BB)} = H_{mn}(\mathbf{0}) = \delta_{mn}\mathcal{E}_n. \tag{5.1.15}$$

Thus H_{AA} and H_{BB} will be equal as the energy of the orbitals is site independent.

$$H^{AA(BB)} = \begin{bmatrix} \mathcal{E}_{2s} & 0 & 0 \\ 0 & \mathcal{E}_{2p_x} & 0 \\ 0 & 0 & \mathcal{E}_{2p_y} \end{bmatrix}. \tag{5.1.16}$$

The matrix elements of the matrices sitting at the anti-diagonal are sums of expectation values of orbitals residing on NN lattice sites. They represent the energy associated with the different bindings and the overlap of the orbitals, respectively. These quantities are highly important as they are responsible for the strong in-plane binding of graphene. For the Hamiltonian matrix, the matrix elements are given by equation (5.1.3) and read

$$h_{mn}^{AB} = \sum_j e^{i\mathbf{k}\boldsymbol{\delta}_j^A} H_{m,n}(\boldsymbol{\delta}_j^A) \qquad \text{and} \qquad h_{mn}^{BA} = \sum_j e^{i\mathbf{k}\boldsymbol{\delta}_j^B} H_{m,n}(\boldsymbol{\delta}_j^B), \tag{5.1.17}$$

where $\{m,n\} = \{2s, 2p_x, 2p_y\}$. The structure is similar for the overlap matrix, and the elements can be obtained from the above equations by substituting $H_{m,n}(\boldsymbol{\delta}_j^{A(B)}) \to S_{m,n}(\boldsymbol{\delta}_j^{A(B)})$. To obtain the details of the matrix elements, the case where a site from sublattice A is interacting with its three NN belonging to sublattice B is investigated. In the following, matrix elements of H^{AB}

are calculated, however the elements of S^{AB} are directly obtained by substituting the energy constants with the overlap constants. Using equations (5.1.7) and (5.1.8), the six unique $H_{m,n}(\boldsymbol{\delta}_j^A)$ become:

$$\begin{aligned}
\left\langle \phi_{2s}^A(\mathbf{r}-\mathbf{R}^B)\middle| H \middle|\phi_{2s}^B(\mathbf{r}-\mathbf{R}^A)\right\rangle &= H_{ss\sigma} \\
\left\langle \phi_{2s}^A(\mathbf{r}-\mathbf{R}^B)\middle| H \middle|\phi_{2p_x}^B(\mathbf{r}-\mathbf{R}^A)\right\rangle &= H_{sp\sigma}\cos(\theta) \\
\left\langle \phi_{2s}^A(\mathbf{r}-\mathbf{R}^B)\middle| H \middle|\phi_{2p_y}^B(\mathbf{r}-\mathbf{R}^A)\right\rangle &= H_{sp\sigma}\sin(\theta) \\
\left\langle \phi_{2p_x}^A(\mathbf{r}-\mathbf{R}^B)\middle| H \middle|\phi_{2p_x}^B(\mathbf{r}-\mathbf{R}^A)\right\rangle &= H_{pp\sigma}\cos^2(\theta)+H_{pp\pi}(1-\cos^2(\theta)) \\
\left\langle \phi_{2p_x}^A(\mathbf{r}-\mathbf{R}^B)\middle| H \middle|\phi_{2p_y}^B(\mathbf{r}-\mathbf{R}^A)\right\rangle &= (H_{pp\sigma}-H_{pp\pi})\cos(\theta)\sin(\theta) \\
\left\langle \phi_{2p_y}^A(\mathbf{r}-\mathbf{R}^B)\middle| H \middle|\phi_{2p_y}^B(\mathbf{r}-\mathbf{R}^A)\right\rangle &= H_{pp\sigma}\sin^2(\theta)+H_{pp\pi}(1-\sin^2(\theta))
\end{aligned}$$

The remaining three elements are obtained using the relations $\langle s|H|p\rangle = -\langle p|H|s\rangle$ and $\langle p_1|H|p_2\rangle = \langle p_2|H|p_1\rangle$. Thus the matrix elements of H^{AB} are

$$\begin{aligned}
h_{11}^{AB} &= \sum_{j=1}^{3} e^{i\mathbf{k}\boldsymbol{\delta}_j^A} H_{ss\sigma} = H_{ss\sigma}e^{ik_y a}\left(1+2e^{-i\frac{3}{2}k_y a}\cos\left(\frac{\sqrt{3}}{2}k_x a\right)\right) \\
h_{12}^{AB} &= \sum_{j=1}^{3} e^{i\mathbf{k}\boldsymbol{\delta}_j^A} H_{sp\sigma}\cos(\theta_j) \\
&= H_{sp\sigma}\left(\cos\left(-\frac{\pi}{6}\right)e^{i\left(\frac{\sqrt{3}}{2}k_x-\frac{1}{2}k_y\right)}+\cos\left(-\frac{5\pi}{6}\right)e^{-i\left(\frac{\sqrt{3}}{2}k_x+\frac{1}{2}k_y\right)}\right) \\
&= H_{sp\sigma}\cos\left(\frac{\pi}{6}\right)e^{-i\frac{k_y}{2}}\left(2i\sin\left(\frac{\sqrt{3}}{2}k_x\right)\right) \\
h_{13}^{AB} &= \sum_{j=1}^{3} e^{i\mathbf{k}\boldsymbol{\delta}_j^A} H_{sp\sigma}\sin(\theta_j) \\
&= H_{sp\sigma}\left(\sin\left(\frac{\pi}{2}\right)e^{ik_y}+\sin\left(-\frac{\pi}{6}\right)e^{i\left(\frac{\sqrt{3}}{2}k_x-\frac{1}{2}k_y\right)}+\sin\left(-\frac{5\pi}{6}\right)e^{-i\left(\frac{\sqrt{3}}{2}k_x+\frac{1}{2}k_y\right)}\right) \\
&= H_{sp\sigma}e^{ik_y}\left(1-2\sin\left(\frac{\pi}{6}\right)e^{-i\frac{3}{2}k_y}\cos\left(\frac{\sqrt{3}}{2}k_x\right)\right)
\end{aligned}$$

$$
\begin{aligned}
h_{22}^{AB} &= \sum_{j=1}^{3} e^{i\mathbf{k}\boldsymbol{\delta}_j^A}\left(H_{pp\sigma}\cos^2(\theta_j) + H_{pp\pi}(1-\cos^2(\theta_j))\right) \\
&= H_{pp\sigma}\cos^2\left(\frac{\pi}{6}\right)e^{-i\frac{k_y}{2}}\left(2\cos\left(\frac{\sqrt{3}}{2}k_x\right)\right) \\
&\quad + H_{pp\pi}e^{ik_y}\left(1+2\sin^2\left(\frac{\pi}{6}\right)e^{-i\frac{3}{2}k_y}\cos\left(\frac{\sqrt{3}}{2}k_x\right)\right) \\
h_{23}^{AB} &= \sum_{j=1}^{3} e^{i\mathbf{k}\boldsymbol{\delta}_j^A}\left(H_{pp\sigma} - H_{pp\pi}\right)\cos(\theta)\sin(\theta) \\
&= \left(H_{pp\sigma} - H_{pp\pi}\right)\left[\cos\left(-\frac{\pi}{6}\right)\sin\left(-\frac{\pi}{6}\right)e^{i\left(\frac{\sqrt{3}}{2}k_x - \frac{1}{2}k_y\right)}\right. \\
&\quad \left. + \cos\left(-\frac{5\pi}{6}\right)\sin\left(-\frac{5\pi}{6}\right)e^{-i\left(\frac{\sqrt{3}}{2}k_x + \frac{1}{2}k_y\right)}\right] \\
&= \left(H_{pp\sigma} - H_{pp\pi}\right)\left(\cos\left(\frac{\pi}{6}\right)\sin\left(\frac{\pi}{6}\right)e^{-i\frac{1}{2}k_y}\left(-2i\sin\left(\frac{\sqrt{3}}{2}k_x\right)\right)\right) \\
h_{33}^{AB} &= \sum_{j=1}^{3} e^{i\mathbf{k}\boldsymbol{\delta}_j^A}\left(H_{pp\sigma}\sin^2(\theta) + H_{pp\pi}(1-\sin^2(\theta))\right) \\
&= H_{pp\sigma}e^{ik_y}\left(1+2\sin^2\left(\frac{\pi}{6}\right)e^{-i\frac{3}{2}k_y}\cos\left(\frac{\sqrt{3}}{2}k_x\right)\right) \\
&\quad + H_{pp\pi}\cos^2\left(\frac{\pi}{6}\right)e^{-i\frac{k_y}{2}}\left(2\cos\left(\frac{\sqrt{3}}{2}k_x\right)\right)
\end{aligned}
$$

The three remaining are matrix elements are $h_{21}^{AB} = -h_{12}^{AB}$, $h_{31}^{AB} = -h_{13}^{AB}$ and $h_{32}^{AB} = h_{23}^{AB}$. The last two submatrices are obtained by Hermitian conjugation, $H^{BA} = \left(H^{AB}\right)^\dagger$ and $S^{BA} = \left(S^{AB}\right)^\dagger$.

5.1.4 The band structure

Having determined the Hamiltonian and overlap matrices, the secular equation (3.1.12) can be solved. The values for the energies associated with bind-

ing and the overlap matrix elements are chosen according to [40]

$$\begin{aligned} H_{sp\sigma} &= 5.5\,eV & S_{sp\sigma} &= -0.10 \\ H_{ss\sigma} &= -6.7\,\text{eV} & S_{ss\sigma} &= 0.20 \\ H_{pp\sigma} &= 5.1\,\text{eV} & S_{pp\sigma} &= -0.15 \\ H_{pp\pi} &= -3.1\,\text{eV} & S_{pp\pi} &= 0.12. \end{aligned} \tag{5.1.18}$$

In Ref [40], these parameter values have been obtained by fitting tight-binding model to experimental data of the band structure in the high symmetry directions ($\Gamma - M - K - \Gamma$). A numerical solver[1] for generalized eigenvalue problems have been used to obtain the band structure. Note that the band structure associated with the anti-bonds is omitted in this thesis. The resulting bands are plotted over the first Brillouin zone in Figure 5.1.2.

A first note is that the electron band structure are six-fold symmetric, which is reasonable as the honeycomb lattice is made up of two triangular lattices. Further, all the bands are centred around the centre of the first Brillouin zone, either being concave with the centre as the maximum of the band or convex with the centre as the minimum. Typically, the band structure is presented in the high symmetry directions, which is shown in Figure 5.1.3.

[1] Here the generalized Schur decomposition from the scientific C++ library *Armadillo* was used.

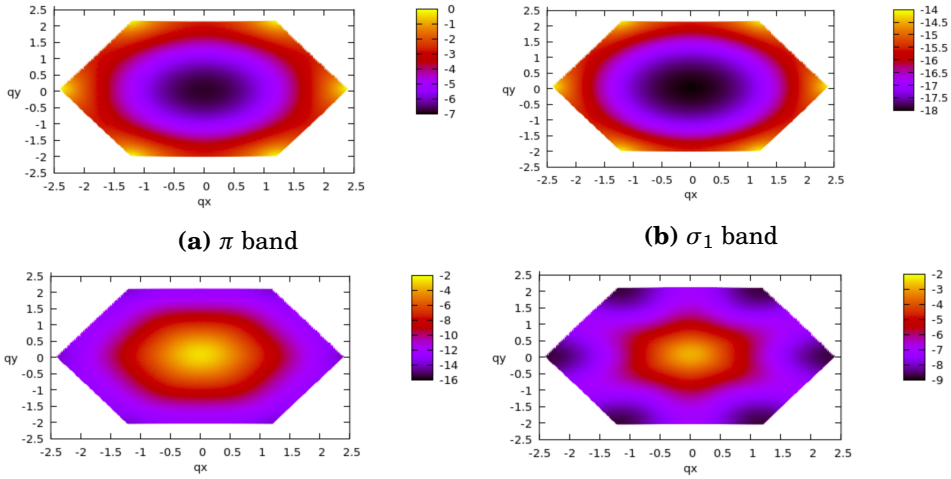

(a) π band

(b) σ_1 band

(c) σ_2 band

(d) σ_3 band

Figure 5.1.2: The four electron bands are plotted over the first Brillouin zone for parameter values given in equation (5.1.18).

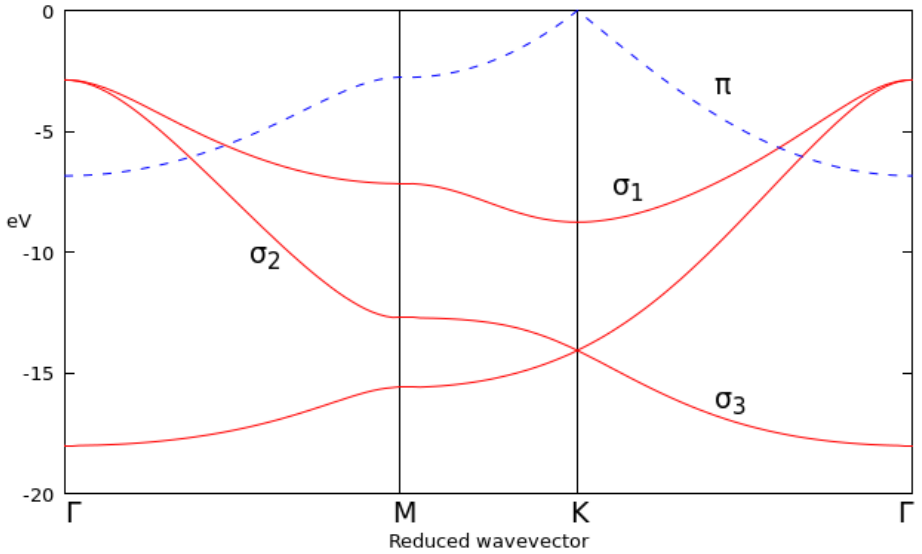

Figure 5.1.3: The band structure of graphene is plotted in the high symmetry directions. The dashed blue line indicates the π band, while the three σ bands are plotted as red solid lines. The four bands associated with anti-bonding are not included in the plot.

Even though a simple NN tight-binding model has been used, the band structure is in good agreement with band structures obtained using more advanced methods [41, 42]. Investigating Figure 5.1.3 an important observation is that two of the σ bands intersect the π band. As a consequence, quasiparticles in the vicinity of the intersections are able to jump from one band to another due to phonon scattering, which is investigated section 5.3.

5.2 The phonon dispersion

The phonon dispersion is determined by the eigenvalues of the dynamic matrix (3.2.15), a scaled Fourier transform of the force-constant matrix. To

be able to obtain an analytic expression, it is assumed that ions couple up to NNN. As both atoms of the unit cell of graphene is carbon, the masses in equation (3.2.14) are equal, however, units have been chosen such that $M = 1$.

In section 5.2.1, the dynamic matrix is specialized to account for vibrations in graphene. Derivations of analytical expressions for the eigenvalues and eigenvectors are presented in sections 5.2.2 and 5.2.3, respectively for the out-of-plane and in-plane phonon modes. Finally, in section 5.2.4, the phonon dispersion is plotted over the first Brillouin zone and in the high symmetry directions.

5.2.1 Adapting the dynamic matrix to graphene

To have a well-defined eigenvalue problem, the basis $c = \left[x^A, y^A, x^B, y^B, z^A, z^B\right]^T$ is chosen in equation (3.2.15). The motivation behind grouping the z vibrations at the end is that the force constants associated with a mix of in-plane and out-of-plane movement, e.g. Φ_{xz} and Φ_{yz}, are zero due to the reflection $z \to -z$ [43]. As a consequence, there is no coupling between in-plane and out-of-plane movement, which makes the dynamic matrix block diagonal

$$D(\mathbf{q}) = \begin{bmatrix} D_{\text{in-plane}}(\mathbf{q}) & 0 \\ 0 & D_{zz}(\mathbf{q}) \end{bmatrix}, \tag{5.2.1}$$

where $D_{\text{in-plane}}(\mathbf{q})$ and $D_{zz}(\mathbf{q})$ are matrices of sizes of sizes 4×4 and 2×2, respectively.

The matrix elements of the dynamic matrix are given by equation (3.2.14). Due to the structure of the basis, both $D_{\text{in-plane}}(\mathbf{q})$ and $D_{zz}(\mathbf{q})$ will be on the form

$$\begin{bmatrix} D_{\mu\nu}^{AA}(\mathbf{q}) & D_{\mu\nu}^{AB}(\mathbf{q}) \\ D_{\mu\nu}^{BA}(\mathbf{q}) & D_{\mu\nu}^{BB}(\mathbf{q}) \end{bmatrix}, \tag{5.2.2}$$

where $\{\mu, \nu\} = \{\{x, y\}, \{z, z\}\}$ and the matrix elements are either 2×2 matrices or scalars. The labels $\{C_1, C_2\} = \{A, B\}$ and $\mu\nu$ is to be interpreted as the

coupling between the movement in μ direction for a fixed lattice site C_1 and the movement in ν direction for all the sites of type C_2.

As the force constants are non-zero up to NNN, the sum in equation (3.2.14) is majorly simplified as it is bounded from above. Thus elements of the dynamic matrix with mixed sublattice lables are single-handedly obtained by summing over NN sites

$$D_{\mu\nu}^{AB(BA)}(\mathbf{q}) = \sum_{j=1}^{3} \Phi_{\mu\nu}^{AB(BA)}(\boldsymbol{\delta}_j^{A(B)}) e^{i\mathbf{q}\boldsymbol{\delta}_j^{A(B)}}, \tag{5.2.3}$$

where $\boldsymbol{\delta}^{A(B)}$ is given by equation (4.1.1). The elements stemming from coupling of lattices sites of the same sublattice are

$$D_{\mu\nu}^{AA(BB)}(\mathbf{q}) = \Phi_{\mu\nu}^{AA(BB)}(\mathbf{0}) + \sum_{j=1}^{6} \Phi_{\mu\nu}^{AA(BB)}(\boldsymbol{\gamma}_j) e^{i\mathbf{q}\boldsymbol{\gamma}_j}, \tag{5.2.4}$$

where $\boldsymbol{\gamma}$ is given by equation (4.1.2) and $\mathbf{0}$ is the null vector. The first term is the force constant associated with movement in μ and ν directions of the same lattice site. The stability condition for the system is [43]

$$\Phi_{\mu\nu}^{AA(BB)}(\mathbf{0}) + 6\Phi_{\mu\nu}^{AA(BB)}(\boldsymbol{\gamma}_j) + 3\Phi_{\mu\nu}^{AB(BA)}(\boldsymbol{\delta}_j^{A(B)}) = 0, \tag{5.2.5}$$

which can be used to eliminate $\Phi_{\mu\nu}^{AA(BB)}(\mathbf{0})$ by substitution. Note that a requirement for $\Phi_{\mu\nu}^{AA(BB)}(\mathbf{0})$ to be non-zero is $\mu \neq \nu$.

5.2.2 Out-of-plane modes

The eigenvalue problem for the out-of-plane vibrations reads

$$\omega^2 = \begin{bmatrix} z^A & z^B \end{bmatrix} \begin{bmatrix} \Phi_{zz}^{AA}(\mathbf{q}) & \Phi_{zz}^{AB}(\mathbf{q}) \\ \Phi_{zz}^{BA}(\mathbf{q}) & \Phi_{zz}^{BB}(\mathbf{q}) \end{bmatrix} \begin{bmatrix} z^A \\ z^B \end{bmatrix}, \tag{5.2.6}$$

where the matrix elements are given by equations (5.2.3) and (5.2.4). As the force constants, $\Phi_{\mu\nu}^{ii'}(j')$, are only dependent on the distance between the lattice sites, it is natural to introduce the constants

$$\alpha_z = \phi^{AB(BA)}(\boldsymbol{\delta}_j^{A(B)}) \qquad \text{and} \qquad \gamma_z = \phi^{AA(BB)}(\boldsymbol{\gamma}_j), \tag{5.2.7}$$

where $\boldsymbol{\delta}_j^{A(B)}$ and $\boldsymbol{\gamma}_j$ are any of the vectors linking the lattice site with its NN or NNN, respectively. The diagonal matrix elements are

$$\begin{aligned} \Phi_{zz}^{AA(BB)}(\mathbf{q}) &= \Phi_{zz}^{AA(BB)}(\mathbf{0}) + \sum_{j=1}^{6} \Phi_{zz}^{AA(BB)}(\boldsymbol{\gamma}_j) e^{i\mathbf{q}\boldsymbol{\gamma}_j} \\ &= 2\gamma_z \left(2\cos\left(\frac{\sqrt{3}a}{2} q_x \right) \cos\left(\frac{3a}{2} q_y \right) + \cos\left(\sqrt{3} a q_x \right) - 3 \right) - 3\alpha_z, \end{aligned} \tag{5.2.8}$$

where the substitution from equation (5.2.5) with $\{\mu, \nu\} = \{z, z\}$ has been used, going from the first to the second line. To obtain the off-diagonal elements, note that $\sum_j e^{i\mathbf{q}\boldsymbol{\delta}_j^B} = \sum_j e^{-i\mathbf{q}\boldsymbol{\delta}_j^A}$.

$$\begin{aligned} \Phi_{zz}^{AB}(\mathbf{q}) &= \alpha_z \sum_{j=1}^{3} e^{i\mathbf{q}\boldsymbol{\delta}_j^A} = \alpha_z e^{iq_y} \left(1 + 2e^{-i\frac{3}{2}q_y} \cos\left(\frac{\sqrt{3}}{2} q_x \right) \right) \\ \Phi_{zz}^{BA}(\mathbf{q}) &= \alpha_z \sum_{j=1}^{3} e^{i\mathbf{q}\boldsymbol{\delta}_j^B} = \alpha_z \sum_{j=1}^{3} e^{-i\mathbf{q}\boldsymbol{\delta}_j^A} = \left(\Phi_{zz}^{AB}(\mathbf{q}) \right)^* \end{aligned} \tag{5.2.9}$$

Having established the matrix elements, the eigenvalues of the dynamic matrix are

$$\begin{aligned} \omega_{\mathrm{ZO}} &= \sqrt{\Phi_{zz}^{AA}(\mathbf{q}) + |\Phi_{zz}^{AB}(\mathbf{q})|} \\ \omega_{\mathrm{ZA}} &= \sqrt{\Phi_{zz}^{AA}(\mathbf{q}) - |\Phi_{zz}^{AB}(\mathbf{q})|}, \end{aligned} \tag{5.2.10}$$

with eigenvectors

$$\frac{1}{\sqrt{2}}\begin{bmatrix} -\sqrt{\frac{\Phi_{zz}^{AB}(\mathbf{q})}{\Phi_{zz}^{AB}(\mathbf{q})^*}} & 1 \\ \sqrt{\frac{\Phi_{zz}^{AB}(\mathbf{q})}{\Phi_{zz}^{AB}(\mathbf{q})^*}} & 1 \end{bmatrix}. \tag{5.2.11}$$

Note that all the elements of the eigenvectors have equal modulus. As the operators which diagonalize the system are formed by a linear combination of the original basis using the entries of each row of the eigenvectors as weights, one concludes that the vibrational out-of-plane modes are either symmetrical or anti-symmetrical. This justifies labelling the eigenvalues $\omega_{\mathrm{ZO,ZA}}$, where Z denotes that it corresponds to vibration in the z direction and A and O denotes whether the mode is acoustical(symmetric) or optical(anti-symmetric). The acoustical phonons are responsible for vibrations where the graphene sheet vibrates as a whole unit, while the optical describe vibrations where the two sublattices vibrate out of phase. Thus it is understandable that the acoustical phonons are less energetic than the optical. Another observation is that the amplitudes associated with optical phonons must be much smaller than the amplitudes of the acoustical for the graphene sheet not to break.

5.2.3 In-plane modes

The symmetries of the honeycomb lattice impose constraints on the dynamical matrix. To make use of the symmetry properties, the new variables $\xi, \eta = x \pm iy$ are introduced. As each lattice site exhibits three-fold symmetry about the z axis, the effect of C_3 rotations taken at the centre of the unit cell is investigated. The lattice sites transform as

$$\boldsymbol{\delta}_1^{A(B)} \to \boldsymbol{\delta}_2^{A(B)} \to \boldsymbol{\delta}_3^{A(B)}, \qquad \boldsymbol{\gamma}_1 \to \boldsymbol{\gamma}_3 \to \boldsymbol{\gamma}_5 \qquad \text{and} \qquad \boldsymbol{\gamma}_2 \to \boldsymbol{\gamma}_4 \to \boldsymbol{\gamma}_6, \tag{5.2.12}$$

while the new variables undergo the transformation $(\xi, \eta) \to (\xi, \eta)e^{\pm i2\pi/3}$. For a visualization, see Figure 4.1.1.

Due to the new variables, the force constants will transform differently according to the subscripts. Force constants with different subscripts will transform like identity,

$$\Phi^{AB}_{\xi\eta}(\boldsymbol{\delta}^A_1) = \Phi^{AB}_{\xi\eta}(\boldsymbol{\delta}^A_2) = \Phi^{AB}_{\xi\eta}(\boldsymbol{\delta}^A_3), \tag{5.2.13}$$

while the force constants with equal subscripts will transform as covariate variabeles [43], e.g.

$$\begin{aligned} \Phi^{AB}_{\xi\xi}(\boldsymbol{\delta}^A_1) &= \Phi^{AB}_{\xi\xi}(\boldsymbol{\delta}^A_2)e^{i\frac{2\pi}{3}} = \Phi^{AB}_{\xi\xi}(\boldsymbol{\delta}^A_3)e^{-i\frac{2\pi}{3}} \\ \Phi^{AB}_{\eta\eta}(\boldsymbol{\delta}^A_1) &= \Phi^{AB}_{\eta\eta}(\boldsymbol{\delta}^A_2)e^{-i\frac{2\pi}{3}} = \Phi^{AB}_{\eta\eta}(\boldsymbol{\delta}^A_3)e^{i\frac{2\pi}{3}}. \end{aligned} \tag{5.2.14}$$

In this context, the order of partial differentiation is indifferent, thus the force constants which differ with respect to the order of the subscripts are equal, e.g. $\Phi^{AB}_{\eta\xi} = \Phi^{AB}_{\xi\eta}$. For simplified notation the following constants are introduced

$$\begin{aligned} \alpha &= \Phi^{AB}_{\xi\eta}(\boldsymbol{\delta}^A_1) \qquad \beta = \Phi^{AB}_{\xi\xi}(\boldsymbol{\delta}^A_1) \\ \gamma &= \Phi^{AA}_{\xi\eta}(\boldsymbol{\gamma}_1) \qquad \delta = \Phi^{AA}_{\xi\xi}(\boldsymbol{\gamma}_1) = \Phi^{AA}_{\eta\eta}(\boldsymbol{\gamma}_1), \end{aligned} \tag{5.2.15}$$

where δ is complex while the remaining are real [43]. The complex conjugate of δ is $\delta^* = \Phi^{AA}_{\xi\xi}(\boldsymbol{\gamma}_4) = \Phi^{AA}_{\eta\eta}(\boldsymbol{\gamma}_4)$.

The eigenvalue problem to solve is

$$\begin{bmatrix} u^A_\xi & u^A_\eta & u^B_\xi & u^B_\eta \end{bmatrix} \begin{bmatrix} \Phi^{AA}(\mathbf{q}) & \Phi^{AB}(\mathbf{q}) \\ \Phi^{BA}(\mathbf{q}) & \Phi^{BB}(\mathbf{q}) \end{bmatrix} \begin{bmatrix} u^A_\eta \\ u^A_\xi \\ u^B_\eta \\ u^B_\xi \end{bmatrix}. \tag{5.2.16}$$

Note that the basis vectors have different ordering on the two sides of the matrix, which is a consequence of the Hermitian conjugation (as $(u^{A(B)}_\xi)^* = u^{A(B)}_\eta$). Each entry of the matrix is itself a 2×2 matrix, where

$$\Phi^{AA}(\mathbf{q}) = \begin{bmatrix} \Phi^{AA}_{\xi\eta}(\mathbf{q}) & \Phi^{AA}_{\xi\xi}(\mathbf{q}) \\ \Phi^{AA}_{\eta\eta}(\mathbf{q})^* & \Phi^{AA}_{\xi\eta}(\mathbf{q}) \end{bmatrix} \qquad \text{and} \qquad \Phi^{AB}(\mathbf{q}) = \begin{bmatrix} \Phi^{AB}_{\xi\eta}(\mathbf{q}) & \Phi^{AB}_{\xi\xi}(\mathbf{q}) \\ \Phi^{AB}_{\eta\eta}(\mathbf{q}) & \Phi^{AB}_{\xi\eta}(\mathbf{q}) \end{bmatrix}.$$

Next the entries of the matrices above are investigated, starting with the element corresponding to NNN and different subscripts

$$\begin{aligned}\Phi^{AA}_{\xi\eta}(\mathbf{q}) &= \Phi^{AA}_{\xi\eta}(\mathbf{0}) + \sum_{j=1}^{6} \Phi^{AA}_{\xi\eta}(\boldsymbol{\gamma}_j) e^{i\mathbf{q}\boldsymbol{\gamma}_j} \\ &= 2\gamma\left(2\cos\left(\frac{\sqrt{3}a}{2}q_x\right)\cos\left(\frac{3a}{2}q_y\right) + \cos\left(\sqrt{3}aq_x\right) - 3\right) - 3\alpha.\end{aligned} \tag{5.2.17}$$

Equation (5.2.5) was used to eliminate $\Phi^{AA}_{\xi\eta}(\mathbf{0})$, going from the fist to the second line. For the case where the subscripts are equal, the element associated with on-site vibration is zero. Thus the matrix elements are

$$\begin{aligned}\Phi^{AA}_{\xi\xi}(\mathbf{q}) &= \Phi^{AA}_{\xi\xi}(\mathbf{0}) + \sum_{j=1}^{6} \Phi^{AA}_{\xi\xi}(\boldsymbol{\gamma}_j) e^{i\mathbf{q}\boldsymbol{\gamma}_j} = \sum_{j=1}^{3} \Phi^{AA}_{\xi\xi}(\boldsymbol{\gamma}_{(2j-1)}) e^{i\mathbf{q}\boldsymbol{\gamma}_{(2j-1)}} + \Phi^{AA}_{\xi\xi}(\boldsymbol{\gamma}_{2j}) e^{i\mathbf{q}\boldsymbol{\gamma}_{2j}} \\ &= \delta\left(e^{i\sqrt{3}q_x} + e^{i\frac{2\pi}{3}} e^{i\left(-\frac{\sqrt{3}}{2}q_x + \frac{3}{2}q_y\right)} + e^{-i\frac{2\pi}{3}} e^{-i\left(\frac{\sqrt{3}}{2}q_x + \frac{3}{2}q_y\right)}\right) \\ &\quad + \delta^*\left(e^{-i\frac{2\pi}{3}} e^{i\left(\frac{\sqrt{3}}{2}q_x + \frac{3}{2}q_y\right)} + e^{-i\sqrt{3}q_x} + e^{i\frac{2\pi}{3}} e^{i\left(\frac{\sqrt{3}}{2}q_x - \frac{3}{2}q_y\right)}\right) \\ &= \delta\left(e^{i\sqrt{3}q_x} + 2\cos\left(\frac{3}{2}q_y + \frac{2\pi}{3}\right) e^{-i\frac{\sqrt{3}}{2}q_x}\right) + \delta^*\left(e^{-i\sqrt{3}q_x} + 2\cos\left(\frac{3}{2}q_y - \frac{2\pi}{3}\right) e^{i\frac{\sqrt{3}}{2}q_x}\right)\end{aligned} \tag{5.2.18}$$

$$\begin{aligned}\Phi^{AA}_{\eta\eta}(\mathbf{q}) &= \sum_{j=1}^{3} \Phi^{AA}_{\eta\eta}(\boldsymbol{\gamma}_{(2j-1)}) e^{i\mathbf{q}\boldsymbol{\gamma}_{(2j-1)}} + \Phi^{AA}_{\eta\eta}(\boldsymbol{\gamma}_{2j}) e^{i\mathbf{q}\boldsymbol{\gamma}_{2j}} \\ &= \delta\left(e^{i\sqrt{3}q_x} + e^{-i\frac{2\pi}{3}} e^{i\left(-\frac{\sqrt{3}}{2}q_x + \frac{3}{2}q_y\right)} + e^{+i\frac{2\pi}{3}} e^{-i\left(\frac{\sqrt{3}}{2}q_x + \frac{3}{2}q_y\right)}\right) \\ &\quad + \delta^*\left(e^{+i\frac{2\pi}{3}} e^{i\left(\frac{\sqrt{3}}{2}q_x + \frac{3}{2}q_y\right)} + e^{i\sqrt{3}q_x} + e^{i\frac{2\pi}{3}} e^{i\left(\frac{\sqrt{3}}{2}q_x - \frac{3}{2}q_y\right)}\right) \\ &= \delta\left(e^{i\sqrt{3}q_x} + 2\cos\left(\frac{3}{2}q_y - \frac{2\pi}{3}\right) e^{-i\frac{\sqrt{3}}{2}q_x}\right) + \delta^*\left(e^{-i\sqrt{3}q_x} + 2\cos\left(\frac{3}{2}q_y + \frac{2\pi}{3}\right) e^{i\frac{\sqrt{3}}{2}q_x}\right).\end{aligned} \tag{5.2.19}$$

Note that $\Phi^{AA}_{\eta\eta}(\mathbf{q}) = \left(\Phi^{AA}_{\xi\xi}(\mathbf{q})\right)^*$. Next the matrix elements associated with NN are calculated. First out is the element with different subscripts

$$\Phi^{AB}_{\xi\eta}(\mathbf{q}) = \sum_{j=1}^{3} \Phi^{AB}_{\xi\eta}(\boldsymbol{\delta}^A_j) e^{i\mathbf{q}\boldsymbol{\delta}^A_j} = \alpha e^{iq_y}\left(1 + 2e^{-i\frac{3}{2}q_y}\cos\left(\frac{\sqrt{3}}{2}q_x\right)\right). \tag{5.2.20}$$

For the elements with equal subscripts the only difference is how $\Phi^{AB}_{\eta\eta}(\boldsymbol{\delta}^A_j)$ transforms

$$\begin{aligned}\Phi^{AB}_{\xi\xi}(\mathbf{q}) &= \sum_{j=1}^{3} \Phi^{AB}_{\xi\xi}(\boldsymbol{\delta}^A_j) e^{i\mathbf{q}\boldsymbol{\delta}^A_j} \\ &= \beta\left(e^{iq_y} + e^{i\frac{2\pi}{3}} e^{-i\left(\frac{\sqrt{3}}{2}q_x + \frac{1}{2}q_y\right)} + e^{-i\frac{2\pi}{3}} e^{i\left(\frac{\sqrt{3}}{2}q_x - \frac{1}{2}q_y\right)}\right) \\ &= \beta e^{iq_y}\left(1 + 2e^{-i\frac{3}{2}q_y}\cos\left(\frac{\sqrt{3}}{2}q_x - \frac{2\pi}{3}\right)\right)\end{aligned} \tag{5.2.21}$$

$$\begin{aligned}\Phi^{AB}_{\eta\eta}(\mathbf{q}) &= \sum_{j=1}^{3} \Phi^{AB}_{\eta\eta}(\boldsymbol{\delta}^A_j) e^{i\mathbf{q}\boldsymbol{\delta}^A_j} \\ &= \beta\left(e^{iq_y} + e^{-i\frac{2\pi}{3}} e^{-i\left(\frac{\sqrt{3}}{2}q_x + \frac{1}{2}q_y\right)} + e^{i\frac{2\pi}{3}} e^{i\left(\frac{\sqrt{3}}{2}q_x - \frac{1}{2}q_y\right)}\right) \\ &= \beta e^{iq_y}\left(1 + 2e^{-i\frac{3}{2}q_y}\cos\left(\frac{\sqrt{3}}{2}q_x + \frac{2\pi}{3}\right)\right).\end{aligned} \tag{5.2.22}$$

The matrix elements associated with the B sublattice are obtained from the matrix elements from the A sublattice with the transformation $(x, y) \to -(x, y)$. Note that the phase obtained for the force-constants under transformation will switch sign due to the mirror symmetry about the x-axis. Hence the matrix elements for the B sublattice are:

$$\begin{aligned}\Phi^{BB}_{\xi\eta}(\mathbf{q}) &= \Phi^{AA}_{\xi\eta}(\mathbf{q}) & \Phi^{BA}_{\xi\eta}(\mathbf{q}) &= \Phi^{AB}_{\xi\eta}(\mathbf{q})^* \\ \Phi^{BB}_{\xi\xi}(\mathbf{q}) &= \Phi^{AA}_{\xi\xi}(\mathbf{q})^* & \Phi^{BA}_{\xi\xi}(\mathbf{q}) &= \Phi^{AB}_{\eta\eta}(\mathbf{q})^* \\ \Phi^{BB}_{\eta\eta}(\mathbf{q}) &= \Phi^{AA}_{\eta\eta}(\mathbf{q})^* & \Phi^{BA}_{\eta\eta}(\mathbf{q}) &= \Phi^{AB}_{\xi\xi}(\mathbf{q})^*.\end{aligned} \tag{5.2.23}$$

For further simplified notation, the following constants are introduced

$$\begin{aligned} a &= \Phi^{AA}_{\xi\eta}(\mathbf{q}) & d &= \Phi^{AB}_{\xi\xi}(\mathbf{q}) \\ b &= \Phi^{AA}_{\xi\xi}(\mathbf{q}) & e &= \Phi^{AB}_{\eta\eta}(\mathbf{q}). \\ c &= \Phi^{AB}_{\xi\eta}(\mathbf{q}) \end{aligned} \tag{5.2.24}$$

Hence the eigenvalue problem can neatly be stated

$$\begin{bmatrix} u^A_\xi & u^A_\eta & u^B_\xi & u^B_\eta \end{bmatrix} \begin{bmatrix} a & b & c & d \\ b^* & a & e & c \\ c^* & e^* & a & b^* \\ d^* & c^* & b & a \end{bmatrix} \begin{bmatrix} u^A_\eta \\ u^A_\xi \\ u^B_\eta \\ u^B_\xi \end{bmatrix}. \tag{5.2.25}$$

The eigenvalues[2] are the roots of the polynomial $\lambda^4 + A\lambda^3 + B\lambda^2 + C\lambda + D$, where the coefficients are

$$\begin{aligned} A &= -4a \\ B &= 6a^2 - 2(|b|^2 + |c|^2) - |d|^2 - |e|^2 \\ C &= 2a(2(-a^2 + |b|^2 + |c|^2) + |d|^2 + |e|^2) - (b + b^*)(cd^* + c^*d + ce^* + c^*e) \\ D &= a^4 - a^2\left(2(|b|^2 + |c|^2) + |d|^2 + |e|^2\right) + a(b + b^*)(cd^* + c^*d + ce^* + c^*e) \\ &\quad + |b|^4 + |c|^4 - (c^*)^2de - c^2e^*d^* - |c|^2(b^2 + (b^*)^2) - |b|^2(d^*e + e^*d) + |d|^2|e|^2. \end{aligned}$$

The roots are

[2] The eigenvalues have been obtained using *Wolphram Mathematica*

$$\begin{aligned}
\omega_{\mathrm{LA}}^2 &= -\frac{A}{2} - \frac{1}{2}\sqrt{\kappa} + \frac{1}{2}\sqrt{\frac{3A^2}{4} - 2B - \kappa - \frac{\lambda}{4\sqrt{\kappa}}} \\
\omega_{\mathrm{TA}}^2 &= -\frac{A}{2} - \frac{1}{2}\sqrt{\kappa} - \frac{1}{2}\sqrt{\frac{3A^2}{4} - 2B - \kappa - \frac{\lambda}{4\sqrt{\kappa}}} \\
\omega_{\mathrm{LO}}^2 &= -\frac{A}{2} + \frac{1}{2}\sqrt{\kappa} + \frac{1}{2}\sqrt{\frac{3A^2}{4} - 2B - \kappa + \frac{\lambda}{4\sqrt{\kappa}}} \\
\omega_{\mathrm{TO}}^2 &= -\frac{A}{2} + \frac{1}{2}\sqrt{\kappa} - \frac{1}{2}\sqrt{\frac{3A^2}{4} - 2B - \kappa + \frac{\lambda}{4\sqrt{\kappa}}},
\end{aligned} \tag{5.2.26}$$

where the following quantities have been introduced (all defined in terms of the coefficients of the polynomial):

$$\begin{aligned}
\epsilon &= B^2 - 3AC + 12D \\
\zeta &= 2B^3 - 9ABC + 27C^2 + 27A^2D - 72BD \\
\theta &= \zeta + \sqrt{-4\epsilon^3 + \zeta^2} \\
\kappa &= \frac{A^2}{4} - \frac{2B}{3} + \frac{1}{3}\left(\frac{2^{1/3}\epsilon}{\theta^{1/3}} + \frac{\theta^{1/3}}{2^{1/3}}\right) \\
\lambda &= -A^3 + 4AB - 8C.
\end{aligned}$$

The in-plane eigenvalues are labelled **L**ongitudinal or **T**ransversal and **A**coustical or **O**ptical to indicate which phonon mode they are related to. The corresponding eigenvectors are

$$S = \begin{bmatrix} E_1/J_1 & F_1/J_1 & G_1/J_1 & 1 \\ E_2/J_2 & F_2/J_2 & G_2/J_2 & 1 \\ E_3/J_3 & F_3/J_3 & G_3/J_3 & 1 \\ E_4/J_4 & F_4/J_4 & G_4/J_4 & 1 \end{bmatrix} \tag{5.2.27}$$

where the quantities used to define the different components are

$$
\begin{aligned}
E_i &= ba^2 - ace^* - 2ab\omega_i^2 + b(\omega_i^2)^2 + b^*(|c|^2 - b^2) + bde^* + ce^*\omega_i^2 + cd^*(\omega_i^2 - a) \\
F_i &= \left((a-\omega_i^2)^2 - |d|^2\right)(\omega_i^2 - a) - c^*\left(c(\omega_i^2 - a) + bd\right) - b^*\left(b(\omega_i^2 - a) + cd^*\right) \\
G_i &= d(c^*)^2 - (b+b^*)(a-\omega_i^2)c^* + |b|^2 d^* + e^*\left((\omega_i^2 - a)^2 - |d|^2\right) \\
J_i &= c^*(a^2 + b^2 - |c|^2 + (\omega_i^2)^2 - 2a\omega_i^2) + be^*(\omega_i^2 - a) + d^*(\omega_i^2 b + ce^* - ab).
\end{aligned}
$$

Keep in mind that the in-plane dispersion has been obtained using the transformed variables $\eta, \xi = x \pm iy$. To decompose the eigenvectors onto the Cartesian directions, observe that the transformed variables relate to the original as

$$
\begin{bmatrix} u_\eta^A \\ u_\xi^A \\ u_\eta^B \\ u_\xi^B \end{bmatrix} = \begin{bmatrix} 1 & -i & 0 & 0 \\ 1 & 1 & 0 & 0 \\ 0 & 0 & 1 & -i \\ 0 & 0 & 1 & i \end{bmatrix} \begin{bmatrix} x^A \\ y^A \\ x^B \\ y^B \end{bmatrix}. \tag{5.2.28}
$$

Let the transformation matrix be denoted T. Then the eigenvectors for the original basis, which can be interpreted in terms of Cartesian directions, are obtained by the matrix product ST.

5.2.4 The phonon dispersion

The phonon dispersion is given by the positive square roots of the eigenvalues of the vibrational modes. Values for the constants associated with the force-constant matrix, given by equations (5.2.7) and (5.2.24), are chosen according to [43]

$$
\begin{aligned}
\alpha &= -4.046 & \gamma &= 1.107 \\
\gamma &= -0.238 & \alpha_z &= -1.176 \\
\beta &= -1.096 & \gamma_z &= 0.190,
\end{aligned} \tag{5.2.29}
$$

where all values are in units of $10^5\,\mathrm{cm}^{-2}$. The dispersions are plotted over the first Brillouin zone in Figure 5.2.1, where they are in units of eV.

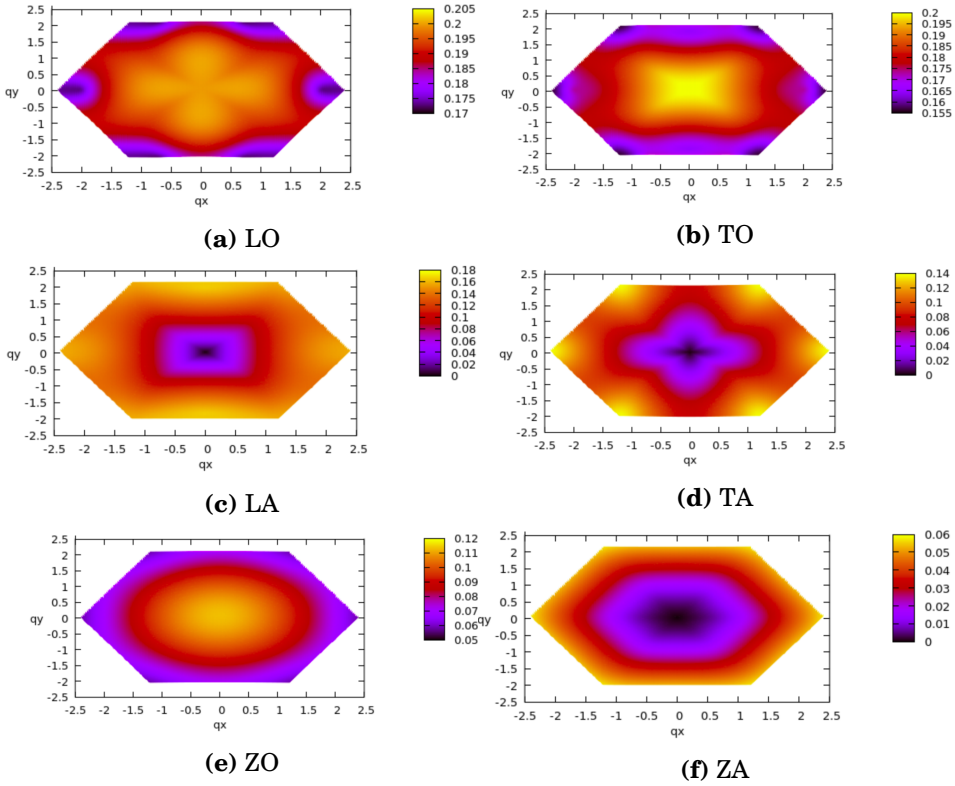

Figure 5.2.1: The six phonon dispersions of the system are plotted over the first Brillouin zone for parameter values given by equation (5.2.29). The dispersions are in units of electron volts.

A highly interesting observation is the four-fold symmetry present in the in-plane dispersions near the centre of the Brillouin zone. From intuition one would suspect three- or six-fold symmetry due to the geometry of the lattice.

The phonon dispersions along the high symmetry directions are shown in Figure 5.2.2. Even though a simple nearest neighbour interaction model has been used, the dispersions are in good quantitatively agreement with

results obtained from more advanced methods [44, 45]. However, the simple model does not capture all details of the dispersion, thus a model including more than NNN interactions might be more suited. During the last days of work with the thesis, the author became aware that a model considering interactions up to the third nearest neighbours is able to capture the details of the phonon dispersion [46].

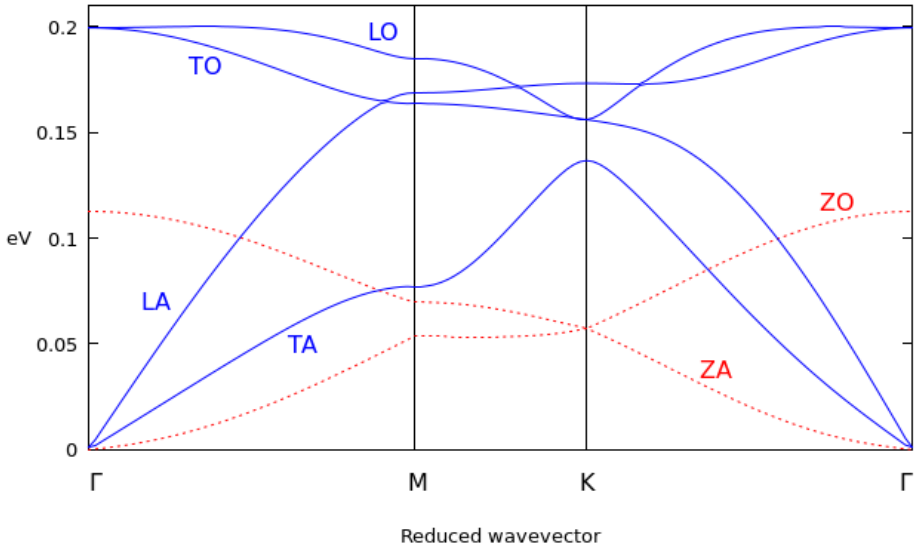

Figure 5.2.2: The phonon dispersion is plotted in the high symmetry directions. The dashed red lines indicate the acoustical (ZA) and optical (ZO) out-of-plane modes, while the solid blue lines show the in-plane modes. The four in-plane modes are LA, TA, LO and TO, corresponding to either **L**ongitudinal or **T**ransversal and **A**coustical or **O**ptical.

5.3 Electron-phonon coupling

The electron-phonon coupling is investigated in the low temperature limit (~ 100 K), in which the thermal energy (≈ 9 meV) is much smaller than the typical energy associated with phonons ≈ 190 meV [47]. Thus phonon emission is assumed to dominate phonon absorption and to be the only source of electron scattering.

In section 5.3.1, the quantities involved in the electron-phonon coupling constant derived in section 3.3 are presented. Section 5.3.2 provides restrictions to the EPC constant, forcing it to be physically acceptable. Finally, in section 5.3.3, the total EPC of the different bands is investigated as a function of the Fermi energy.

5.3.1 Adapting electron-phonon coupling to graphene

The general expression for the electron-phonon coupling constant is given by equation (3.3.10). Hence the quantities $\mathbf{W}^{\alpha\beta}_{\mathbf{k},\mathbf{k}+\mathbf{q}}$, $\omega_{\mathbf{q}\lambda}$ and $\mathbf{e}_\lambda(\mathbf{q})$ are needed in order to calculate the EPC constant. The two latter are the phonon dispersion and its eigenvectors, as presented in section 5.2.1. The remaining quantity, $\mathbf{W}^{\alpha\beta}_{\mathbf{k},\mathbf{k}+\mathbf{q}}$, is related to the electrons and given by equation (3.3.6). The spatial part of the Bloch functions, $u^\alpha_{\mathbf{k}}$, is obtained as a linear combination of the basis used in the tight-binding model

$$u^\alpha_{\mathbf{k}}(\mathbf{r}) = \sum_{i=1}^{8} w^\alpha_{i\mathbf{k}} \phi_i(\mathbf{r}), \tag{5.3.1}$$

where the basis is given by equation (5.1.1). The weights, $w^\alpha_{i\mathbf{k}}$, are the eigenvectors associated with the eigenvalues $\mathcal{E}^\alpha_{\mathbf{k}}$ and are obtained by solving the secular equation (3.1.12). The index i runs over the columns while α gives the row index. Each row is normalized according to $\sum_{i=1}^{8} |w^\alpha_{i\mathbf{k}}|^2 = 1$.

The orbitals are shaped as damped exponentials and require a value for the Bohr radius. As discussed in section 4.2, a suitable value for the Bohr radius is $r_B = a/10$, where a denotes the lattice constant.

5.3.2 Derivation of electron-phonon coupling constants

As the electron-phonon coupling is restricted to the low temperature limit and only phonon emission is considered, some constraints are imposed on the coupling constant. Let $(\mathbf{k}\alpha)$ denote a quasiparticle of momentum $\mathbf{k}$ in band α and $(\mathbf{q}\lambda)$ a phonon of momentum $\mathbf{q}$ in mode λ. Then the general scattering process as presented in Figure 3.3.1 is specialized to the case where an incident quasiparticle in state $(\mathbf{k}\alpha)$ emits a phonon $(\mathbf{q}\lambda)$ and is scattered into state $(\mathbf{k}+\mathbf{q},\beta)$.

By examining the scattering process, constraints on the calculation of the EPC are derived. First it is clear that momentum transfer must be $\mathbf{q}=\mathbf{k}'-\mathbf{k}$ to satisfy conservation of momentum. Secondly, the scattering process is in general inelastic which relates the energies as $\mathcal{E}_{\mathbf{k}\alpha}-\omega_{\mathbf{q}\lambda}\geq\mathcal{E}_{\mathbf{k}'\beta}$. To ensure that the outgoing state is unoccupied initially, the energy of the outgoing state has to satisfy $\mathcal{E}_{\mathbf{k}'\beta}\geq\mathcal{E}_F$, where $\mathcal{E}_F$ is the Fermi energy. Hence $\mathcal{E}_{\mathbf{k}\alpha}-\omega_{\mathbf{q}\lambda}\geq\mathcal{E}_F$, which imposes the constraint $\mathcal{E}_{\mathbf{k}\alpha}\geq\mathcal{E}_F$, as only phonon emission is considered. Thus the EPC constant, as given by equation (3.3.10), is redefined to

$$g^{\alpha\beta\lambda}_{\mathbf{k},\mathbf{k}+\mathbf{q}}\rightarrow g^{\alpha\beta\lambda}_{\mathbf{k},\mathbf{k}+\mathbf{q}}\theta\left(\mathcal{E}_{\mathbf{k}\alpha}-\mathcal{E}_{\mathbf{k}+\mathbf{q},\beta}-\omega_{\mathbf{q}\lambda}\right)\theta\left(\mathcal{E}_{\mathbf{k}+\mathbf{q},\beta}-\mathcal{E}_F\right), \tag{5.3.2}$$

where θ denotes the unit step function and conservation of momentum has been ensured by the substitution $\mathbf{k}'=\mathbf{k}+\mathbf{q}$. An interesting quantity is the total probability amplitude of scattering of the incident state $(\mathbf{k}\alpha)$ by phonon mode λ to any state in band β. This total transition probability amplitude is obtained by summing over all momentum transfers

$$g^{\alpha\beta\lambda}_{\mathbf{k}}=\sum_{\mathbf{q}}g^{\alpha\beta\lambda}_{\mathbf{k},\mathbf{k}+\mathbf{q}}\theta\left(\mathcal{E}_{\mathbf{k}\alpha}-\mathcal{E}_{\mathbf{k}+\mathbf{q},\beta}-\omega_{\mathbf{q}\lambda}\right)\theta\left(\mathcal{E}_{\mathbf{k}+\mathbf{q},\beta}-\mathcal{E}_F\right). \tag{5.3.3}$$

Furthermore, to determine the EPC constant as a function of the Fermi energy, the coupling constant is averaged over constant energy contours, where

the energy of the outgoing state lies on the Fermi surface

$$g^{\alpha\beta\lambda}(\mathcal{E}_F) = \frac{1}{N_\beta(\mathcal{E}_F)} \sum_{\mathbf{k}} g_{\mathbf{k}}^{\alpha\beta\lambda} \delta(\mathcal{E}_{\mathbf{k},\beta} - \mathcal{E}_F), \tag{5.3.4}$$

where $N_\beta(\mathcal{E}_F) = \sum_{\mathbf{k}} \delta(\mathcal{E}_{\mathbf{k}\beta} - \mathcal{E}_F)$ is the number of states in band β that lie on the Fermi surface, which also goes by the name density of states.

5.3.3 The coupling constant as a function of $\mathcal{E}_F$

The electron-phonon coupling constant, given by equation (5.3.4), is plotted for different values of the Fermi energy in Figure 5.3.1. As plotting the coupling constant $g^{\alpha\beta\lambda}(\mathcal{E}_F)$ for all α, β and λ would yield 96 contributions for each value of $\mathcal{E}_F$, it has been simplified to, $g^{\alpha\beta\lambda}(\mathcal{E}_F) \rightarrow g^{\alpha}_{\text{inter(intra)}}(\mathcal{E}_F)$. The subscript indicates whether the outgoing state is the same as the incoming state (due to intra-band scattering), or the outgoing state is different (inter-band scattering). In the plot, the components $\sigma_{2,\text{intra}}$ and $\sigma_{1,\text{inter}}$ are left out as their values were unphysical, due to the numerical implementation by the author. This was also the case for the calculated coupling constant corresponding to scattering between bands σ_2 and σ_3, and σ_1 and σ_2. Hence they are not included in the inter-band components of the coupling constants.

As Figure 5.3.1 shows, the coupling constant is rather rough and fluctuate a lot, which is due to the numerical calculation. As computational complexity turns out to be a problem, the discretization of the Fermi energy is limited. The expression for the coupling constant involves δ functions with respect to the Fermi energy, and when its discrete values does not match up with the energy of the bands, the δ function gives zero. Hence the origin of the rough and fluctuating form lies in the finite discretization of the Fermi energy.

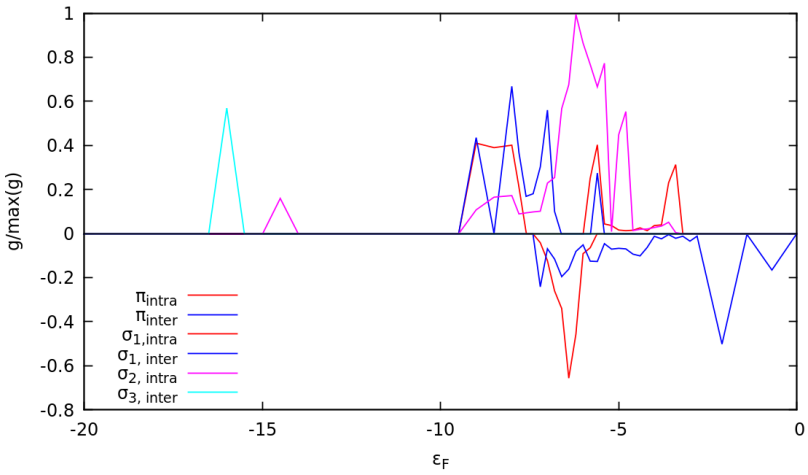

Figure 5.3.1: The electron-phonon coupling constant is plotted as a function of $\mathcal{E}_F$. The coupling constant of each band is divided in two components, accounting for intra and inter band scattering. To easily distinguish the coupling related to incoming states in the π band from the incoming states in the σ bands, the EPC constant of the π band is plotted as a negative value.

As the relative sizes of the EPC constants are comparable, both intra- and inter-band scattering must be considered for all bands. The numerically obtained results showed that the in-plane modes are the main source of the EPC as the contribution from the out-of-plane phonons turned out to be negligible. However, they might couple stronger to the bands described by the coupling constants that were not included due to unphysicallity.

It is interesting to compare the electron-phonon coupling constant with the density of states in the bands, which is plotted in Figure 5.3.2. An interesting observation is how closely the EPC constant follow the DOS. At first sight it might seem a little mysterious, however keeping the physical process of the electron-phonon coupling in mind, it makes sense. As the energies associated with the electron bands are in a much greater range (from -20 eV to 0 eV) than the energies of the phonons (from 0 eV to 0.2 eV), it is clear

that the energy of the outgoing quasiparticle will not be changed much with respect to the incoming. Hence, when summing over all allowed transitions onto a Fermi surface, the resulting coupling constant will basically follow the density of states. Thus, it is clear that the EPC constant is closely connected to the band structure.

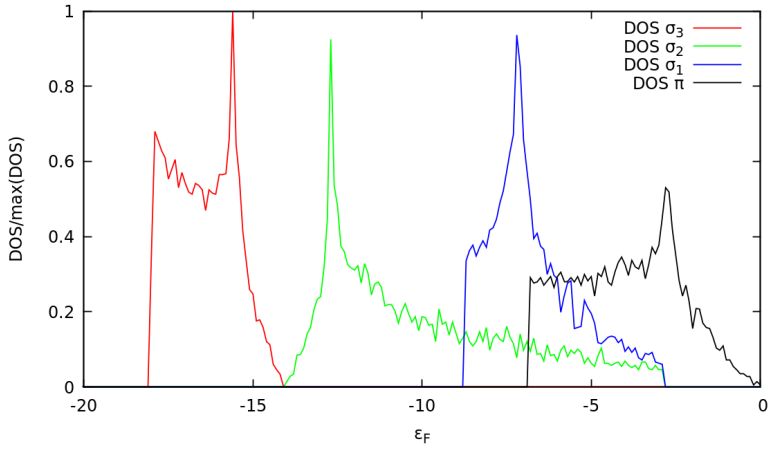

Figure 5.3.2: The density of states is plotted for the four bands as a function of the energy.

With this in mind, a conclusion can be presented in the discussion from section 5.2.4 of whether the phonon model is sufficient or not. It is now clear, in the context of EPC, that the qualitative shape of the phonon dispersion is far more important than the details due to the large energy difference between typical phonon and band energies. Hence one may conclude that the model used for the phonon system, considering up to NNN ion interactions, is sufficient for calculating EPC. However, it is not necessarily sufficient when considering other quantities, as they may be more dependent on the details of the dispersion.

Chapter 6

Concluding remarks

The aim of this Master thesis was to theoretically investigate the electron-phonon coupling in graphene. As it is a fundamental coupling between phonons and electrons, quantities related to both phonons and electrons had to be derived. The main results of the thesis are the electron-phonon coupling constant, the derivation of the phonon dispersion and the calculation of the band structure, all adapted to graphene.

Typically, the EPC constant is labelled by a phonon mode, and thus gives the total probability amplitude of any of the bands being scattered by that mode. In this thesis a more complex expression for the coupling constant has been derived, where it has been given band indices in addition to the phonon mode. Hence the coupling constant gives the transition probability of a quasiparticle in band α with momentum $\mathbf{k}$ being scattered by a phonon of momentum $\mathbf{q}$ in mode λ, either by emission or absorption, to a state $\mathbf{k}+\mathbf{q}$ in band β, where $\{\alpha,\beta\}$ run over the electron bands of the system.

The EPC constant has been investigated in the context of graphene in the low temperature limit, in which phonon emission dominates absorption. The total transition probability amplitude for a quasiparticle in band α to band β, as a function of the Fermi energy, as shown in Figure 5.3.1. It has been

argumented for, and visually supported that the coupling constant is highly correlated with the shape of the DOS of the electron bands. In addition, it has been argumented for that the EPC is more dependent on the band structure than the phonon dispersion.

It would have interesting to investigate the electron-phonon coupling in greater detail. The author would than suggest creating contour plots where the coupling constant is plotted over the first Brillouin zone for different values of the Fermi energy. Especially energies near the peaks of the DOS of the electron bands are of special interest.

The phonon dispersion was found as the eigenvalues of the dynamic matrix (3.2.15) when interactions up to NNN were considered. Due to symmetry constraints, in-plane and out-of-plane vibrations are decoupled. A surprising discovery is that the dispersion of the in-plane modes, when plotted over the first Brillouin zone, exhibits four-fold symmetry. As the honeycomb lattice is two interpenetrating triangular lattices, one would suspect a three-fold, perhaps a six-fold symmetry by intuition. The mechanism behind the four-fold symmetry is not clear to the author.

The electron bands were found by solving the secular equation (3.1.12), resulting in four bands, three σ bands and one π band. A linear combination of the $|2s\rangle, |2p_x\rangle$ and $|2p_y\rangle$ orbitals provide the diagonal band basis for the σ bands, while the diagonal basis for the π band is given by a linear combination of $|2p_z\rangle$ orbitals. Hence the in-plane and z components were decoupled for the bands as well.

Interesting applications of the results in this thesis is calculating the effective electron-electron interaction due to the EPC and calculating the spectral function for the quasiparticles of the bands. A derivation of the effective interaction is provided in the notes by R. Heid [48], where the EPC constant is a central quantity. By calculating the effective interaction for the different bands, it is possible to determine which bands that will display superconductivity as a function of the Fermi energy.

Bibliography

[1] T. E. of Encyclopaedia Britannica, "Pencil | writing implement," 2017. [Online]. Available: https://www.britannica.com/technology/pencil-writing-implement

[2] Novoselov, K. S., Geim, A. K., Morozov, S. V., Jiang, D., Zhang, Y., Dubonos, S. V., Grigorieva, I. V., and Firsov, A. A., "Electric Field Effect in Atomically Thin Carbon Films," *Science*, vol. 306, no. 5696, pp. 666–669, 2004. [Online]. Available: http://science.sciencemag.org/content/306/5696/666

[3] Geim, A. K. and Novoselov, K. S., "The rise of graphene," *Nature Materials*, vol. 6, pp. 183 EP –, Mar 2007. [Online]. Available: http://dx.doi.org/10.1038/nmat1849

[4] Lee, C., Wei, X., Kysar, J. W., and Hone, J., "Measurement of the Elastic Properties and Intrinsic Strength of Monolayer Graphene," *Science*, vol. 321, no. 5887, pp. 385–388, 2008. [Online]. Available: http://science.sciencemag.org/content/321/5887/385

[5] "Young's Modulus - Tensile and Yield Strength for common Materials ," retrived: May 16, 2018. [Online]. Available: https://www.engineeringtoolbox.com/young-modulus-d_417.html

[6] Balandin, A. A., "Thermal properties of graphene and nanostructured carbon materials," *Nature Materials*, vol. 10, pp. 569 EP –, Jul 2011,

review Article. [Online]. Available: http://dx.doi.org/10.1038/nmat3064

[7] Mayorov, A. S., Gorbachev, R. V., Morozov, S. V., Britnell, L., Jalil, R., Ponomarenko, L. A., Blake, P., Novoselov, K. S., Watanabe, K., Taniguchi, T., and Geim, A. K., "Micrometer-Scale Ballistic Transport in Encapsulated Graphene at Room Temperature," *Nano Letters*, vol. 11, no. 6, pp. 2396–2399, Jun 2011. [Online]. Available: https://doi.org/10.1021/nl200758b

[8] Moser, J., Barreiro, A., and Bachtold, A., "Current-induced cleaning of graphene," *Applied Physics Letters*, vol. 91, no. 16, p. 163513, 2007. [Online]. Available: https://doi.org/10.1063/1.2789673

[9] Bunch, J. S., Verbridge, S. S., Alden, J. S., van der Zande, A. M., Parpia, J. M., Craighead, H. G., and McEuen, P. L., "Impermeable Atomic Membranes from Graphene Sheets," *Nano Letters*, vol. 8, no. 8, pp. 2458–2462, 2008, pMID: 18630972. [Online]. Available: https://doi.org/10.1021/nl801457b

[10] Shiraz, H. and Tavakoli, O., "Investigation of graphene-based systems for hydrogen storage," *Renewable and Sustainable Energy Reviews*, vol. 74, pp. 104 – 109, 2017. [Online]. Available: http://www.sciencedirect.com/science/article/pii/S136403211730271X

[11] Ruse, E., Buzaglo, M., Pri-Bar, I., Shunak, L., Nadiv, R., Pevzner, S., Siton-Mendelson, O., Skripnyuk, V., Rabkin, E., and Regev, O., "Hydrogen storage kinetics: The graphene nanoplatelet size effect," *Carbon*, vol. 130, pp. 369 – 376, 2018. [Online]. Available: http://www.sciencedirect.com/science/article/pii/S0008622318300125

[12] Castro Neto, A. H. , Guinea, F. , Peres, N. M. R. , Novoselov, K. S. , and Geim, A. K., "The electronic properties of graphene," *Rev. Mod. Phys.*, vol. 81, pp. 109–162, Jan 2009. [Online]. Available: https://link.aps.org/doi/10.1103/RevModPhys.81.109

[13] Akhmerov, A. , "Electron-phonon interaction," 2017.

[14] Morozov, S., Novoselov, K., and Geim, A., "Electronic transport in graphene," *Phys. Usp.*, vol. 51, no. 7, pp. 744–748, 2008. [Online]. Available: https://ufn.ru/en/articles/2008/7/h/

[15] Novoselov, K. S., Jiang, Z., Zhang, Y., Morozov, S. V., Stormer, H. L., Zeitler, U., Maan, J. C., Boebinger, G. S., Kim, P., and Geim, A. K., "Room-Temperature Quantum Hall Effect in Graphene," *Science*, vol. 315, no. 5817, pp. 1379–1379, 2007. [Online]. Available: http://science.sciencemag.org/content/315/5817/1379

[16] Fuhrer, M. S., Lau, C. N., and MacDonald, A. H., "Graphene: Materially Better Carbon, volume=35, doi=10.1557/mrs2010.551," *MRS Bulletin*, no. 4, p. 289–295, 2010.

[17] Cao, Y., Fatemi, V., Fang, S., Watanabe, K., Taniguchi, T., Kaxiras, E., and Jarillo-Herrero, P., "Unconventional superconductivity in magic-angle graphene superlattices," *Nature*, vol. 556, pp. 43 EP –, Mar 2018, article. [Online]. Available: http://dx.doi.org/10.1038/nature26160

[18] Cao, Y., Fatemi, V., Demir, A., Fang, S., Tomarken, S. L., Luo, J. Y., Sanchez-Yamagishi, J. D., Watanabe, K., Taniguchi, T., Kaxiras, E., Ashoori, R. C., and Jarillo-Herrero, P., "Correlated insulator behaviour at half-filling in magic-angle graphene superlattices," *Nature*, vol. 556, pp. 80 EP –, Mar 2018. [Online]. Available: http://dx.doi.org/10.1038/nature26154

[19] Mele, E. J., "Novel electronic states seen in graphene," 2018.

[20] Stewart, G. R., "Unconventional superconductivity," *Advances in Physics*, vol. 66, pp. 75–196, Apr. 2017.

[21] "The quantum theory of the emission and absorption of radiation," *Proceedings of the Royal Society of London A: Mathematical, Physical and Engineering Sciences*, vol. 114, no. 767, pp. 243–265, 1927. [Online]. Available: http://rspa.royalsocietypublishing.org/content/114/767/243

[22] Fetter, A. and Walecka, J.D., *Quantum Theory of Many-Particle Systems*. Mineola, New York: Dover Publications, inc., 2003.

[23] H. Fröhlich, "Electrons in lattice fields," *Advances in Physics*, vol. 3, pp. 325–361, Jul. 1954.

[24] Bloch, F., *Z.Phys*, vol. 52, 1928.

[25] Jones, H., Mott, N. F., and Skinner, H. W. B., "A Theory of the Form of the X-Ray Emission Bands of Metals," *Phys. Rev.*, vol. 45, pp. 379–384, Mar 1934. [Online]. Available: https://link.aps.org/doi/10.1103/PhysRev.45.379

[26] Slater, J. C. and Koster, G. F., "Simplified LCAO Method for the Periodic Potential Problem," *Phys. Rev.*, vol. 94, pp. 1498–1524, Jun 1954. [Online]. Available: https://link.aps.org/doi/10.1103/PhysRev.94.1498

[27] Kittel, C., *Introduction to Solid State Physics*, 8th ed. New York: John Wiley & Sons, Inc., 2005.

[28] Pickett, W. E., ""Tight Binding" Method: Linear Combination of Atomic Orbit als (LCAO," Lecture notes: Condensed Matter Physics, PHY 240A, 2013.

[29] Bloch, F., "Über die Quantenmechanik der Elektronen in Kristallgittern," *Zeitschrift für Physik*, vol. 52, no. 7, pp. 555–600, Jul 1929. [Online]. Available: https://doi.org/10.1007/BF01339455

[30] Cardona, M., "Phonons: The second type of quantum excitations discovered," *Annalen der Physik*, vol. 9, no. 11-12, pp. 865–870. [Online]. Available: https://onlinelibrary.wiley.com/doi/abs/10.1002/1521-3889%28200011%299%3A11/12%3C865%3A%3AAID-ANDP865%3E3.0.CO%3B2-G

[31] Tamm, I.G., *Z. Phys*, vol. 60, pp. 345–363, 1930.

[32] Mott, N.F., "Wave mechanics: Elementary theory. by j. frenkel. pp. viii, 278. 20s. 1932. (oxford; at the clarendon press)," *The Mathematical Gazette*, vol. 17, no. 223, p. 135–136, 1933.

[33] Fujita, S., Ito. K., and Godoy, S. , *Quantum Theory of Conducting Matter*. Springer-Verlag New York, 2009.

[34] Sudbø, A., "Lecture notes in kvanteteorien for faste stoffer," 2017.

[35] Razeghi, M., *Electron Phonon Interactions*. Boston, MA: Springer US, 2009, pp. 1–10. [Online]. Available: https://doi.org/10.1007/978-0-387-92168-6_14

[36] Peschel, G., "Carbon-Carbon bonds: Hybridization," Lecture notes: Physics of Nanoscale Carbon, 2013.

[37] Hemmer, P.C., *Kvantemekanikk*, 5th ed. Trondheim: Tapir Akademisk Forlag, 1980.

[38] Blinder, S. M., "Chapter 7: The hydrogen atom," 2002.

[39] Jena, D. , "Handout 11," 2015, lecture notes ECE 4070. [Online]. Available: https://courses.cit.cornell.edu/mse5470/handout11.pdf

[40] Gharekhanlou, B. and Khorasani, S., "An overview of tight-binding method for two-dimensional carbon structures," pp. 1–36, 01 2012.

[41] Kogan, E. and Nazarov, V. U., "Symmetry classification of energy bands in graphene," *Phys. Rev. B*, vol. 85, p. 115418, Mar 2012. [Online]. Available: https://link.aps.org/doi/10.1103/PhysRevB.85.115418

[42] Latil, S. and Henrard, L., "Charge Carriers in Few-Layer Graphene Films," *Phys. Rev. Lett.*, vol. 97, p. 036803, Jul 2006. [Online]. Available: https://link.aps.org/doi/10.1103/PhysRevLett.97.036803

[43] Falkovsky, L.A., "Phonon dispersion in graphene," *Soviet Journal of Experimental and Theoretical Physics*, vol. 105, pp. 397–403, Aug. 2007.

[44] Koukaras, E. N., Kalosakas, G., Galiotis, C., and Papagelis, K., "Phonon properties of graphene derived from molecular dynamics simulations," *Scientific Reports*, vol. 5, pp. 12 923 EP –, Aug 2015, article. [Online]. Available: http://dx.doi.org/10.1038/srep12923

[45] Yan, J.-A., Ruan, W. Y., and Chou, M. Y., "Phonon dispersions and vibrational properties of monolayer, bilayer, and trilayer graphene: Density-functional perturbation theory," *Phys. Rev. B*, vol. 77, p. 125401, Mar 2008. [Online]. Available: https://link.aps.org/doi/10.1103/PhysRevB.77.125401

[46] Falkovsky, L. A., "Symmetry constraints on phonon dispersion in graphene," *Physics Letters A*, vol. 372, pp. 5189–5192, Jul. 2008.

[47] Mazzola, F., Wells, J. W., Yakimova, R., Ulstrup, S., Miwa, J. A., Balog, R., Bianchi, M., Leandersson, M., Adell, J., Hofmann, P., and Balasubramanian, T., "Kinks in the σ Band of Graphene Induced by Electron-Phonon Coupling," *Phys. Rev. Lett.*, vol. 111, p. 216806, Nov 2013. [Online]. Available: https://link.aps.org/doi/10.1103/PhysRevLett.111.216806

[48] Heid, R., "Electron-Phonon Coupling," Institute for Solid State Physics, Karlsruhe Institute of Technology. [Online]. Available: https://www.cond-mat.de/events/correl17/manuscripts/heid.pdf